The Astrophysical Journal, 877:60 (30pp), 2019 May 20 https://doi.org/10.3847/1538-4357/ab1018

The Elusive Majority of Young Moving Groups. I. Young Binaries and Lithium-rich Stars in the Solar Neighborhood

Brendan P. Bowler[1,11,12], Sasha Hinkley[2], Carl Ziegler[3], Christoph Baranec[4], John E. Gizis[5], Nicholas M. Law[6], Michael C. Liu[7], Viyang S. Shah[1], Evgenya L. Shkolnik[8], Basmah Riaz[9], and Reed Riddle[10]

[1] Department of Astronomy, The University of Texas at Austin, Austin, TX 78712, USA; bpbowler@astro.as.utexas.edu
[2] University of Exeter, Physics and Astronomy, Exeter EX4 4QL, UK
[3] Dunlap Institute for Astronomy and Astrophysics, University of Toronto, Toronto, ON M5S 3H4, Canada
[4] Institute for Astronomy, University of Hawaiʻi at Mānoa, 640 N. A'ohōkū Place, Hilo, HI 96720, USA
[5] Department of Physics and Astronomy, University of Delaware, Newark, DE 19716, USA
[6] Department of Physics and Astronomy, University of North Carolina at Chapel Hill, Chapel Hill, NC 27599-3255, USA
[7] Institute for Astronomy, University of Hawaiʻi at Mānoa, 2680 Woodlawn Drive, Honolulu, HI 96822, USA
[8] School of Earth and Space Exploration, Arizona State University, Tempe, AZ 85281, USA
[9] Universitäts-Sternwarte München, Ludwig Maximilians Universitat, Scheinerstraße 1, D-81679 München, Germany
[10] California Institute of Technology, 1200 E. California Boulevard, Pasadena, CA 91125, USA

Received 2018 June 25; revised 2019 February 11; accepted 2019 March 1; published 2019 May 24

Abstract

Young stars in the solar neighborhood serve as nearby probes of stellar evolution and represent promising targets to directly image self-luminous giant planets. We have carried out an all-sky search for late-type (≈K7–M5) stars within 100 pc selected primarily on the basis of activity indicators from the *Galaxy Evolution Explorer* and *ROSAT*. Approximately 2000 active and potentially young stars are identified, of which we have followed up over 600 with low-resolution optical spectroscopy and over 1000 with diffraction-limited imaging using Robo-AO at the Palomar 1.5 m telescope. Strong lithium is present in 58 stars, implying ages spanning ≈10–200 Myr. Most of these lithium-rich stars are new or previously known members of young moving groups including TWA, β Pic, Tuc-Hor, Carina, Columba, Argus, AB Dor, Upper Centaurus Lupus, and Lower Centaurus Crux; the rest appear to be young low-mass stars without connections to established kinematic groups. Over 200 close binaries are identified down to 0$''$.2—the vast majority of which are new—and will be valuable for dynamical mass measurements of young stars with continued orbit monitoring in the future.

Key words: binaries: visual – stars: low-mass

Supporting material: machine-readable tables

1. Introduction

Since the initial recognition of young moving groups (YMGs) about two decades ago (e.g., Kastner et al. 1997; Torres et al. 2000; Zuckerman & Webb 2000), these nearby associations of intermediate-age (≈10–200 Myr) stars have been the subject of increasing interest in the stellar, substellar, and exoplanet communities (e.g., Torres et al. 2008; Bowler 2016; Mamajek 2016b). These loose, relatively sparse ($N\sim$ 50–300), kinematically comoving groups in the solar neighborhood ($\lesssim$100 pc) provide a link between the youngest T Tauri stars and the older population of field stars.

Because of their proximity and youth, YMGs have become a rich resource to study a broad range of topics: the evolution of stellar dynamos and activity (e.g., Shkolnik & Barman 2014; Ansdell et al. 2015), dynamical masses of intermediate-age stars (e.g., Close et al. 2005; Montet et al. 2015; Nielsen et al. 2016; Janson et al. 2018), the structure and evolution of debris disks (e.g., Wyatt et al. 2015), young brown dwarfs and free-floating planetary-mass objects (Allers & Liu 2013; Liu et al. 2013, 2016; Gagné et al. 2014; Aller et al. 2016; Faherty et al. 2016), multiplicity at young ages (Best et al. 2017; Janson et al. 2017; Shan et al. 2017), and the initial mass function of sparse clusters (Gagné et al. 2017). Members of YMGs have also become favored targets for direct imaging searches for exoplanets (e.g., Biller et al. 2013; Brandt et al. 2014; Bowler et al. 2015a; Chauvin et al. 2015) and, as a result, many of the known directly imaged planets and planetary-mass companions orbit members of these associations (e.g., 2M1207–3932b, Chauvin et al. 2004; HR 8799bcde, Marois et al. 2008; β Pic b, Lagrange et al. 2010; 51 Eri b, Macintosh et al. 2015; GU Psc b, Naud et al. 2014; 2M2236+4751b, Bowler et al. 2017). However, the relatively limited number of bona fide members of YMGs—a few hundred confirmed using fully constrained space motions together with other independent youth indicators—has gradually become a barrier to measuring more precise occurrence rates with direct imaging and searching for correlations with stellar host mass (Bowler & Nielsen 2018).

Despite numerous dedicated searches to identify nearby young stars, the current census of stellar and substellar members of YMGs is vastly incomplete. Assuming a standard initial mass function, Kraus et al. (2014), Gagné et al. (2017), and Shkolnik et al. (2017) find that tens to hundreds of low-mass stars and brown dwarfs are probably missing from membership lists of Tuc-Hor, TWA, and β Pic. The same is likely to be true of other YMGs owing to early, biased searches for bright members using *Hipparcos* parallaxes and proper motions. This has prompted a number of programs to find new low-mass members spanning the stellar and substellar mass

[11] Visiting astronomer, Kitt Peak National Observatory, National Optical Astronomy Observatory, which is operated by the Association of Universities for Research in Astronomy (AURA) under a cooperative agreement with the National Science Foundation.

[12] Visiting astronomer, Cerro Tololo Inter-American Observatory, National Optical Astronomy Observatory, which is operated by the Association of Universities for Research in Astronomy (AURA) under a cooperative agreement with the National Science Foundation.

regimes (Gizis 2002; Lépine & Simon 2009; Shkolnik et al. 2009, 2017; Schlieder et al. 2010, 2012b; Malo et al. 2013, 2014a; Gagné et al. 2014; Kraus et al. 2014; Riedel et al. 2014, 2017; Binks & Jeffries 2015; Aller et al. 2016). In spite of these innovative efforts, hundreds of low-mass members likely await discovery.

Motivated by the need for additional targets for high-contrast imaging, we have carried out a broad search for low-mass stars in YMGs. The goals of this program are highly focused: to identify new, single, relatively bright ($R \lesssim 15$ mag) YMG members with large proper motions. This facilitates the rapid discrimination of background stars from bound companions for follow-up high-contrast imaging observations. Our strategy is to initially use X-ray and UV activity together with color and proper motion cuts to locate candidate young early-M dwarfs. Having begun this study prior to *Gaia* data releases, our approach to selecting targets for follow-up observations has relied only on proper motions and sky positions without the advantage of having parallaxes.

This study focuses on the characterization of potential young stars and moving group members based on low-resolution optical spectroscopy together with adaptive optics imaging with Robo-AO at the Palomar 60 inch (1.5 m) telescope. In a separate paper, we will present radial velocities from new high-resolution spectroscopy of several hundred potential moving group members as part of a follow-up kinematic analysis. Section 2 summarizes the activity, color, and proper motion cuts used to define our starting sample. Our observations and analysis are described in Sections 3 and 4. Moving group candidates are discussed in Section 5, and our conclusions are summarized in Section 6.

2. Sample Selection

Our starting sample draws from two large catalogs of low-mass stars. The Frith et al. (2013) list of bright M dwarfs ($K < 9$ mag) consists of stars between K7 and M4 selected from the PPMXL catalog (Roeser et al. 2010). The authors applied a series of optical and NIR color cuts to isolate late spectral types, and reduced proper motions are used to distinguish dwarfs from bright, distant giants. Frith et al. required a signal-to-noise ratio (S/N) of at least 5 for proper motions and removed regions surrounding the galactic plane ($|b| < 15°$) susceptible to source confusion. Finally, they combined their list with the Lépine & Gaidos (2011) catalog of bright M dwarfs to produce a final catalog of 8479 late-K to mid-M dwarfs.

We also utilize the Haakonsen & Rutledge (2009) list of *ROSAT* All-Sky Survey Bright Source Catalog (Voges et al. 1999) detections cross-matched with the Two Micron All Sky Survey (2MASS) Point Source Catalog (Cutri et al. 2003; Skrutskie et al. 2006). The authors provide probabilities that each X-ray source is uniquely associated with a near-infrared counterpart. Altogether, 18,497 *ROSAT* detections have non-zero probabilities of being associated with a 2MASS source. For this study, we select 6084 targets with >90% association probabilities as a supplementary catalog to search for young active M dwarfs.

Both samples are then cross-matched against all-sky photometric and proper motion surveys. Near-infrared *J*-, *H*-, and K_S-band photometry are extracted from 2MASS (Skrutskie et al. 2006) with a search radius (R_S) of 5″; r'-band photometry is from the Carlsberg Meridian Catalogue 14 (Evans et al. 2002; $R_S = 5''$); $R2$ magnitudes are from USNO-B1.0 (Monet et al. 2003; $R_S = 5''$); NUV and far-UV photometry are from the latest *Galaxy Evolution Explorer* (*GALEX*) General Release (GR6/GR7; Martin et al. 2005; Morrissey et al. 2007; $R_S = 10''$); *W1*, *W2*, *W3*, and *W4* photometry from the *Wide-field Infrared Survey Explorer*, Wright et al. 2010; $R_S = 10''$); X-ray count rates and hardness ratios are from the *ROSAT* All-Sky Survey Bright Source Catalog (Voges et al. 1999) or, if not detected there, then the *ROSAT* All-Sky Faint Source Catalog (Voges et al. 2000; $R_S = 30''$); and *V*-band magnitudes and proper motions are from the USNO CCD Astrograph Catalog 4 (Zacharias et al. 2013; $R_S = 5''$). If there are multiple *GALEX* detections for the same search position at different epochs, then we adopt the weighted mean and uncertainty of these measurements.

We apply a series of color, activity, proper motion, and photometric distance cuts to both catalogs that are specifically designed to identify nearby young M dwarfs for follow-up planet searches with direct imaging. These criteria are primarily intended for the Haakonsen & Rutledge (2009) catalog (hereinafter HR09), which has a diverse mix of nonstellar "contaminants" (active galactic nuclei, cataclysmic variables, galaxy clusters, etc.). On the other hand, the Frith et al. (2013) catalog (hereinafter F13) is well-vetted for M dwarfs, but these are overwhelmingly expected to be old inactive field stars. Below we list the additional filters we have applied to both samples:

1. Optical brightness cut. Stars with $r' > 15$ mag are excluded. This corresponds to the approximate faintness limit for natural guide star AO instruments like Keck/NIRC2, ensuring an optically bright sample for the possibility of follow-up high-contrast imaging. If no r' measurement is listed in CMC14, then we adopt the $R2$ magnitude from USNO-B1.0 and apply the same brightness cut.
2. Photometric distance cut. *V*-band photometric distance estimates are computed using the M_V versus V–K_S band polynomial fit to Pleiades stars in Bowler et al. (2013). Most known moving groups are located within about 100 pc, so we further restrict our search catalog to photometric distances <100 pc. Photometric distances will underestimate the true distances for binaries and young stars still descending along the Hayashi track, but this cut excludes most of the distant M dwarfs from the sample.
3. Near-infrared color cuts. A series of near-infrared color cuts are imposed to further isolate late-K and early-M dwarfs. Only stars with *J*-band, *H*-band, and K_S-band photometric uncertainties below 0.1 mag are considered. *Hipparcos* K7V–M3V stars and the Lépine & Gaidos (2011) sample of bright M dwarfs are used to establish typical near-infrared colors of M dwarfs (Figure 1). Based on this locus, we impose the following color cuts:

$$J - H > -(H - K_S) + 0.65 \text{ mag}, \tag{1}$$

$$J - H < -(H - K_S) + 1.05 \text{ mag}. \tag{2}$$

These cuts are depicted in Figure 1 for two control samples from *Hipparcos* and Lépine & Gaidos (2011), in addition to the F13 and HR09 catalogs we consider in this work. M dwarfs have already been color-selected for the F13 catalog, so this cut predominantly affects the HR09 catalog.

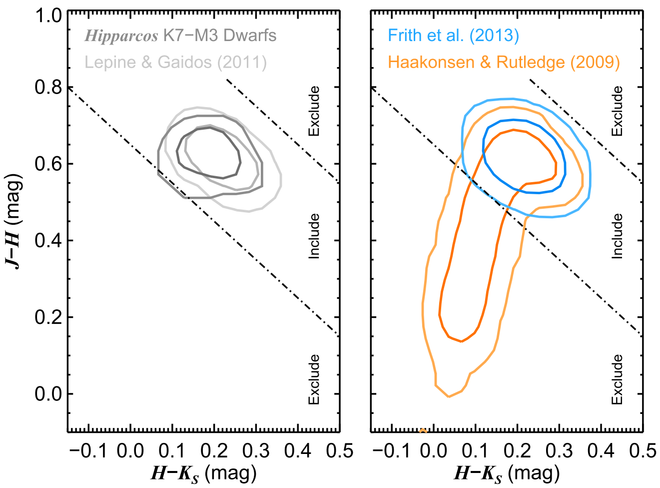

Figure 1. Near-infrared color cuts applied to the F13 and HR09 catalogs to isolate late-K to mid-M dwarfs (dotted–dashed lines). Left: comparison samples of early-M dwarfs from Lépine & Gaidos (2011, light gray) and the XHIP extended compilation of *Hipparcos* stars from Anderson & Francis (2012, dark gray). Right: the F13 catalog (blue) is already selected for M dwarfs, but earlier spectral types are excluded from the HR09 sample (orange) with these color cuts. Contours encompass 68% and 95% of objects with near-infrared photometric uncertainties <0.1 mag.

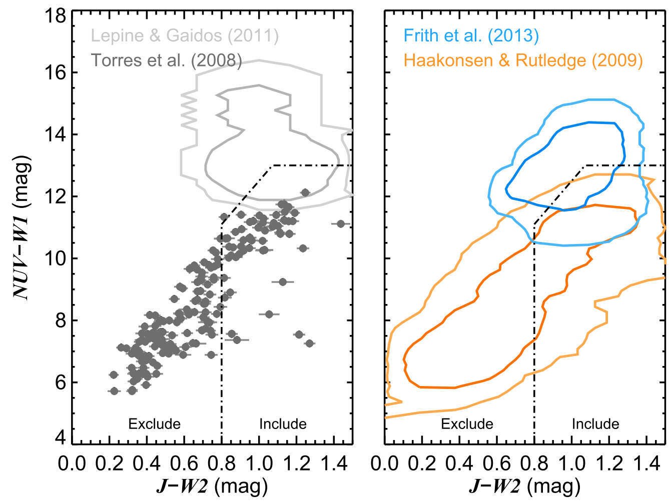

Figure 2. Activity cuts using NUV − $W1$ and J − $W2$ photometry (dotted–dashed lines). Left: comparison sample of field M dwarfs from Lépine & Gaidos (2011) together with the compilation of known YMG members from Torres et al. (2008) spanning 10–150 Myr. Most YMG members trace out a saturated locus of NUV emission compared to the field population at a given J − $W2$ color, which is a proxy for spectral type. Late-K and M dwarfs have J − $W2$ colors $\gtrsim$0.8 mag. Right: our color cuts applied to the F13 and HR09 samples. Most of the F13 M dwarfs are relatively inactive, whereas the HR09 stars are preselected to also exhibit X-ray emission and are therefore also UV bright.

4. UV activity cut. Stars with active chromospheres are readily distinguished from their inactive counterparts using *GALEX* photometry. Following Rodriguez et al. (2013), we use the J – $W2$ versus NUV – $W1$ diagram to identify active stars (Figure 2):
$$\mathrm{NUV}{-}W1 < 7.0(J - W2) + 5.5\ \mathrm{mag}, \quad (3)$$
$$\mathrm{NUV}{-}W1 < 13\ \mathrm{mag}. \quad (4)$$
Based on the spectral type–color relation from Rodriguez et al. (2013), we also require that J – $W2$ > 0.8 mag to isolate late-type ($\geqslant$K5) stars (Figure 2). Note that this cut does not remove white dwarf–M dwarf binaries, which can share similar UV-to-infrared colors to young, active M dwarfs (Silvestri et al. 2007; Shkolnik et al. 2011).
5. Reduced proper motion cut. Reduced proper motions provide a convenient way to separate fast-moving dwarfs from kinematically slow but luminous giants. Following F13, we require $H_K > 6.0$, where the reduced proper motion is $H_K = K + 5\,\log(\sqrt{(\mu_\alpha\cos(\delta)^2 + \mu_\delta^2})) + 5$; here, $\mu_\alpha\cos(\delta)$ and μ_δ are the star's proper motion in arcseconds per year. Finally, we also require the total proper motion to be greater than 25 mas yr^{-1} to ensure that candidate planets identified in AO imaging can be distinguished from background stars on short (∼1 yr) timescales.

Cross-matching the resulting filtered F13 and HR09 samples yields 2060 unique targets, which we use as the starting point for our YMG kinematic selection.

3. Observations

To better characterize our starting sample of 2060 activity-selected late-K and early-M dwarfs, we carried out a follow-up observational program to obtain low-resolution optical spectra of these targets using instruments in the northern and southern hemispheres, together with AO imaging with Robo-AO at the Palomar 60 in (1.5 m) telescope in the north. Altogether we acquired 762 optical spectra of 632 stars, plus an additional four nearby stars sharing common proper motions with targets in our sample. We also obtained 1523 AO images of 1011 stars to uncover and characterize close binaries. The broader goals of this program are to identify single young stars for high-contrast imaging, so known binaries from recent high-resolution campaigns (e.g., Janson et al. 2012, 2014a) are deprioritized, leading to an intentionally biased sample, which we note is not easily amenable to multiplicity statistics. Details about the instrument setups and data reduction are discussed below.

3.1. Mayall/RC-Spec

Observations with the RC-Spectrograph mounted on the 4 m Mayall telescope at Kitt Peak were carried out over eight nights on UT 2013 December 29–31, UT 2014 May 21–23, and UT 2015 June 16–17. Altogether, 478 spectra were obtained for 428 stars. The same instrument setup was used for all observing runs: the BL420 grating in conjunction with the GG-495 filter and 1$''$.5 × 98$''$ slit dimensions produced an average resolving power ($R \equiv \lambda/\Delta\ \lambda$) of ≈2600 spanning 6200–9200 Å. The T2KA CCD with a gain of 1.4 e$^-$ ADU^{-1} was used for the 2013 and 2014 runs; the T2KB CCD was used with a gain of 1.9 e$^-$ ADU^{-1} during the 2015 observations. Sky conditions were partly clear with intermittent clouds. The slit was oriented in a fixed north–south direction throughout the nights, which means targets observed at large hour angles suffered from wavelength-dependent slit loss from differential atmospheric refraction (Filippenko 1982). Most targets were observed near transit, but the continuum slopes of some stars are affected by chromatic slit loss. Our observations are detailed in Table 1.

Each image was bias-subtracted, flat-fielded, and corrected for bad pixels. Night sky lines were removed with median subtraction using 25 pixel regions on either side of the science spectrum. The spectrum was then extracted by summing the central 11 pixel region in the spatial direction. Wavelength calibration was carried out with HeNeAr arc lamps acquired

Table 1
Spectroscopic Observations

2MASS Name	Date (UT)	Telescope/ Instrument	Grating	Res. Power	Exp. (s)	Hα EW (Å)[a]	Li EW (Å)[a]	Na EW (Å)[a]	TiO5 Index	Hammer SpT[b]	Vis. SpT[b]
J00022714–4601439	2014 Jun 27	SOAR/Goodman	SYZY400	1800	300	−1.0	⋯	2.2	0.65	M1	M2
J00104302–2039067	2013 Dec 6	SOAR/Goodman	SYZY400	1800	120	−3.5	⋯	3.1	0.48	M3	M3
J00104302–2039067	2013 Dec 6	SOAR/Goodman	RALC1200	5900	240	−3.2	⋯	⋯	0.49	M3	M3
J00114643–1139553	2013 Dec 6	SOAR/Goodman	SYZY400	1800	150	0.3	⋯	3.6	0.75	M0	M0
J00120761–1550327	2013 Dec 31	Mayall/RC-Spec	BL420	2600	30	−3.2	⋯	1.1	0.93	K:	G/K:
J00141709–6139237	2013 Dec 5	SOAR/Goodman	SYZY400	1800	300	−1.7	⋯	3.1	0.52	M2	M3
J00141709–6139237	2013 Dec 5	SOAR/Goodman	RALC1200	5900	500	−1.8	⋯	⋯	0.55	M2	M2
J00144767–6003477	2014 Jun 25	SOAR/Goodman	SYZY400	1800	300	−5.1	⋯	3.4	0.39	M4	M4
J00151561+0247373	2014 Jun 26	SOAR/Goodman	SYZY400	1800	240	0.4	⋯	1.3	0.88	K5	K7
J00153670–2946003	2013 Dec 5	SOAR/Goodman	SYZY400	1800	300	−9.2	⋯	3.5	0.34	M4	M5

Notes.
[a] Negative values indicate emission. Uncertainties are estimated to be 10% of the quoted values.
[b] Spectral types from `Hammer` have been shown to have a systematic offset of about one spectral subclass for cool stars. Uncertainties are ±1 subclass. Our visual spectral types are more robust and have uncertainties of ±0.5 subclasses.
[c] Likely SB2.
[d] Visual binary.
[e] Common proper motion companion to a star in the parent sample.

(This table is available in its entirety in machine-readable form.)

three to five times per night. About 30 prominent lines are fit with a quadratic function to derive the pixel-to-wavelength solution. Several early-type spectrophotometric standards from Oke (1990) and Hamuy et al. (1992, 1994) were observed each night to broadly correct the continuum shape for throughput losses from the atmosphere, optics, grating, and CCD.

3.2. SOAR/Goodman Spectrograph

A total of 244 spectra were obtained for 168 stars with the Goodman High-Throughput Spectrograph (Clemens et al. 2004) at the Southern Astrophysical Research (SOAR) 4.1 m telescope located on Cerro Pachón, Chile. The observations spanned nine nights on three observing runs: UT 2013 December 4–7, UT 2014 June 25–28, and UT 2015 February 16. Details about individual observations can be found in Table 1. Our strategy was to first observe with the 400 l mm^{-1} grating ("SYZY400") in the M2 setup with the 0$''$.46 slit, which produces an average resolving power of ≈1800 spanning 5000–9000 Å. For a subset of targets—usually those showing strong Hα emission or hints of Li absorption—we also obtained a spectrum with the 1200 l mm^{-1} grating ("RALC1200") in the M5 setup with the 0$''$.46 slit, which produces an average resolving power of ≈5900 spanning 6250–7500 Å. The slit was rotated to parallactic angle for each target on all nights except UT 2013 December 4–5. All observations were carried out with the GG455 order-blocking filter and the Blue Camera CCD, which imprinted strong fringing redward of about 7000 Å. The detector was read out at 400 kHz with 1 × 1 binning. Quartz lamp flats and arc lamps for wavelength calibration were taken immediately after each science observation at the same position on the sky. At least one spectrophotometric standard was targeted per night.

All observations are reduced using custom scripts. Images are bias-subtracted and corrected for bad pixels. A normalized flat field is created at the same location as the science trace on the CCD and is used to remove pixel-to-pixel variations in the science frame, including most (but not all) of the fringing. Spectra are then optimally extracted following the method described in Horne (1986). Wavelength calibration is carried out by fitting Gaussians to 19 strong emission lines from HgAr for the arc lamp frames using the 400 l mm^{-1} grating, and 11 emission lines from CuHeAr for the arc lamp frames using the 1200 l mm^{-1} grating in pixel space. A fourth-order polynomial fit is used to map pixels to wavelengths in an automated fashion for each target. Finally, the extracted spectrum was divided by a spectrophotometric standard observed on the same night to correct for wavelength-dependent throughput losses.

3.3. UH 2.2 m/SuperNova Integral Field Spectrograph

We acquired low-resolution ($R \approx 1300$) optical spectra for 40 stars on UT 2014 January 19 and 21 with the SuperNova Integral Field Spectrograph (SNIFS) at the University of Hawai'i's 88 in (2.2 m) telescope located on Maunakea, Hawai'i. SNIFS is an integral-field spectrograph that uses a microlens array to disperse a 6$''$ × 6$''$ field of view into two channels spanning 3200–11000 Å (Lantz et al. 2004). Multiple O/B standards were observed on each night. After basic image reduction and rectification into data cubes, each spectrum was extracted and wavelength-calibrated with the SNIFS reduction pipeline (Aldering et al. 2006; Scalzo et al. 2010). Details for each target are listed in Table 1.

3.4. P60/Robo-AO

We obtained 1523 adaptive optics images of 1011 targets from our parent sample of 2060 active stars with Robo-AO at the Palomar 60 in (1.5 m) telescope between 2013 July and 2015 June. Robo-AO is an efficient autonomous adaptive optics system that provides diffraction-limited AO observations at optical wavelengths using an ultraviolet laser for wavefront sensing (Baranec et al. 2013, 2014) and an intelligent queue system for target selection (Riddle et al. 2014).

For each observation, Robo-AO's EMCCD camera produces a data cube typically composed of 256 fast readouts with short exposures. These frames are combined using a shift-and-add pipeline for each observation to produce a final science image with a field of view of 44$''$ × 44$''$ that has been resampled to

Table 2
Robo-AO Observations

2MASS ID	UT Date (Y-M-D)	Filter	Exp. (s)	FWHM (″)
J00055520+4129289	2014 Aug 24	SDSS i'	60	0.28
J00074264+6022543	2013 Oct 25	LP600	120	0.26
J00074264+6022543	2014 Nov 8	SDSS i'	60	0.16
J00080642+4757025	2013 Oct 25	SDSS i'	120	0.20
J00085391+2050252	2013 Oct 24	SDSS i'	120	0.25
J00085391+2050252	2014 Nov 6	SDSS i'	60	0.13
J00114643–1139553	2014 Aug 28	SDSS i'	60	0.26
J00120761–1550327	2014 Aug 29	SDSS i'	60	0.35
J00133841+5245050	2014 Aug 26	SDSS i'	60	0.21
J00133841+5245050	2014 Nov 6	SDSS i'	60	0.13

(This table is available in its entirety in machine-readable form.)

21.6 mas pixel^{-1}, or half the native plate scale (see Law et al. 2014 for details). The plate scale and north orientation are derived from observations of globular clusters taken on observing runs throughout the same time period as these data. Because targets tend to be faint and red, most of our observations are carried out with the SDSS i' filter with integration times of 30–120 s. When possible, we obtained multiple observations of candidate visual binaries to test for common proper motion. Details about our individual observations can be found in Table 2.

FWHM values are calculated using the averaged radial profile of the point-spread function (PSF). When seeing conditions degrade, the shift-and-add procedure locks on to noise spikes and produces a narrow core in the final image. For these images, which would otherwise imply sub-diffraction-limited resolution, we ignore the inner 5 pixels for our FWHM measurement. The typical FWHM is about 0.″18, which compares with the diffraction limit of ≈0.″12 at 750 nm. The median seeing at Palomar Observatory is about 1.″1. A total of 73% of our observations have FWHM < 0.″25 and 11% have FWHM < 0.″15. These measurements are reported in Table 2.

Image performance metrics and contrast curves are generated for each target following Law et al. (2014) and Ziegler et al. (2017). To summarize, AO correction is assessed using PSF core size. Targets are divided into high-, medium-, or low-performance groups, which vary primarily with target brightness and natural seeing conditions.[13] We derived 5σ contrast curves using a Monte Carlo injection-recovery analysis of artificial companions generated from the primary's PSF. Contrast curves from our observations are summarized in Figure 3; we typically reach $\Delta i' \approx 5$ mag at 1″. In Section 4.2, we discuss the visual binaries and fainter candidate companions in our images.

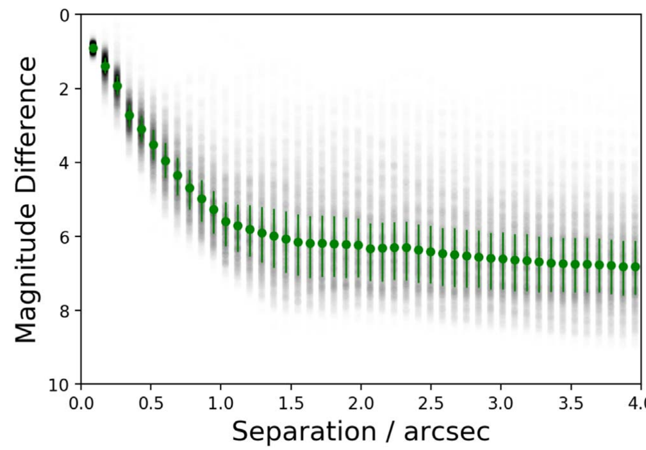

Figure 3. Overview of Robo-AO contrast curves from our observations. 5σ sensitivity limits (overlapping gray circles) are derived using injection-recovery of each star's PSF. The median contrasts and upper and lower quartiles are shown in green.

4. Results

4.1. Spectral Classification

Spectral types are determined using the `Hammer` classification package (Covey et al. 2007), which measures a suite of indices and assigns a spectral type by comparing these values to spectral standards. West et al. (2011) showed that these classifications are generally accurate to ±1 subclass, but for late-M dwarfs there is an average systematic offset of ≈0.4 subtypes toward earlier types. We therefore also assign spectral types using the visual classifying feature in `Hammer`. These two methods are generally in agreement, but our visual types are found to be more reliable, so we adopt an uncertainty of ±0.5 subtypes for these classifications. As expected from our color cuts, the vast majority of objects for which we obtained spectra fall between K5 and M5. Both the automated (index-based) and visual results are reported in Table 1 together with TiO5 indices, which track the onset and strengthening of TiO absorption in the emergent spectra of M dwarfs (Reid et al. 1995).

4.1.1. Hα Emission

Hα emission is observed in the vast majority of our spectra. We measure equivalent widths by fitting a Gaussian function centered at 6563 Å using the curve-fitting package `MPFIT` (Markwardt 2009) and integrating under the best-fit model. Each fit was visually inspected to ensure that the emission-line peak was correctly identified and modeled. Our threshold for clear line emission is < −0.5 Å. For equivalent widths between 0.0 and −0.5 Å, the emission is either very weak or questionable based on visual inspection. Values in this range are less reliable because of the low resolving power of our data and should be treated with caution. High-resolution spectra may be needed to unambiguously search for Hα emission in those stars. Equivalent widths >0 Å indicate that Hα is seen in absorption. Hα line strengths are listed in Table 1. Uncertainties are determined by comparing equivalent widths of the same targets on the same night; we estimate errors of 20% for the quoted line strengths.

Hα equivalent widths are shown as a function of TiO5 index strength in Figure 4. Our targets trace an envelope of Hα emission that increases in strength from about −3 Å at TiO5 values of 0.9 (≈K7) to >10 Å at TiO5 values of 0.4 (≈M4). The shape of this envelope bears a close resemblance to other large spectroscopic samples of M dwarfs (e.g., Riaz et al. 2006; Gaidos et al. 2014; Kraus et al. 2014). Barrado y Navascués & Martin (2003) identified an empirical division that separates accretion-induced Hα emission from saturated chromospheric activity. Eight stars have exceptionally strong Hα emission that falls on or above the saturated chromospheric curve in Figure 4 and may originate in part from disk accretion: 2MASS

[13] Representative contrast curves for each performance group are as follows. High: {0.7, 1.6, 3.9 , 5.5, 6.3, 6.4, 6.4} mag, medium: {0.7, 1.6, 3.2 , 4.4, 5.0, 5.0, 5.0} mag, and low: {0.5, 1.1, 2.2 , 3.1, 3.5, 3.5, 3.5} mag at {0.″1, 0.″2, 0.″5 , 1″, 2″, 3″, 4″}.

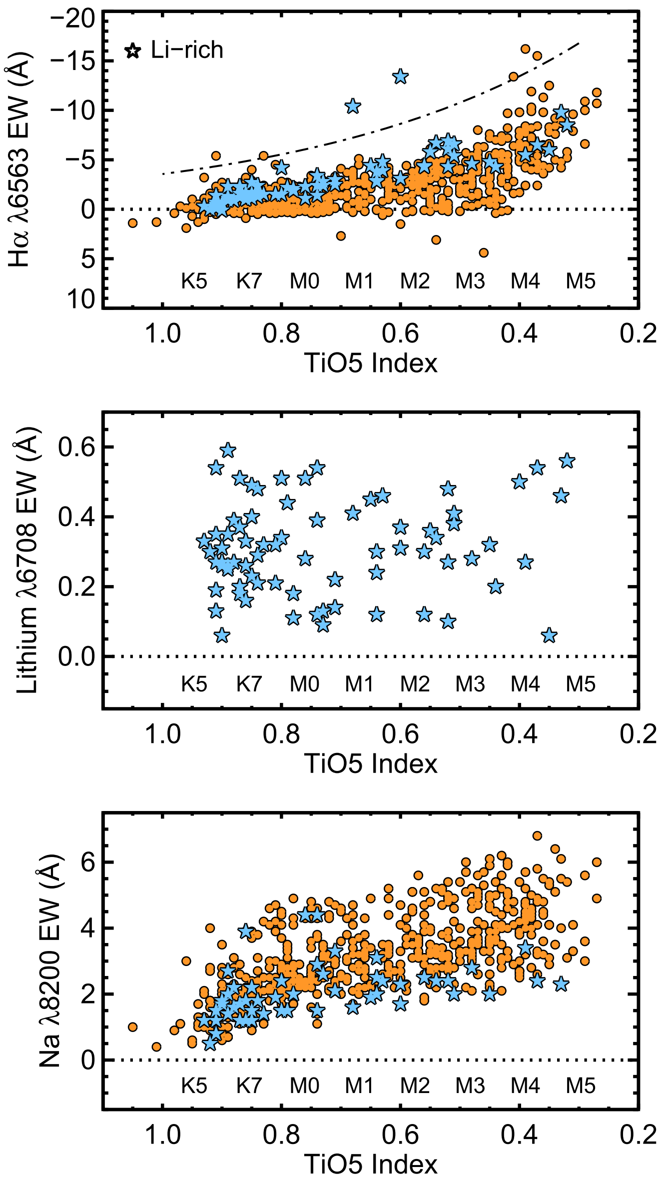

Figure 4. Age and gravity-dependent line strengths from our low-resolution optical spectra. Top panel: Hα equivalent width as a function of TiO5 index strength. The maximum Hα emission from chromospheric activity traces an envelope that increases toward larger equivalent widths at later types. The dotted–dashed curve represents an approximate boundary between saturated chromospheric emission and emission originating from disk accretion identified by Barrado y Navascués & Martin (2003). TiO5 values are converted to spectral types using the relation from Reid et al. (1995). One star, 2MASS J15354856–2958551, has an exceptionally high line strength and lies off the plot. Blue stars denote objects with Li I absorption in their spectra. Middle panel: Li I line strength as a function of TiO5 index strength. A wide range of lithium equivalent widths are apparent, implying ages <100 Myr for these M dwarfs in our sample. Bottom panel: total equivalent width of the gravity-sensitive Na I doublet at ≈8200 Å. Young stars with low surface gravities are expected to have lower sodium strengths.

J10260210–4105537, 2MASS J13314666+2916368, 2MASS J13573397–3139105, 2MASS J14255593+1412101, 2MASS J15354856–2958551, 2MASS J17213497–2152283, 2MASS J18464675+0043260, and 2MASS J19300396–2939322.

4.1.2. Lithium

Li I λ6708 absorption is a well-established indicator of youth in the atmospheres of low-mass stars (e.g., Soderblom et al. 2014). Lithium burning occurs in stellar cores through proton capture reactions at temperatures of about 2.5×10^6 K, and the depletion of lithium among late-type stars with partially or fully convective envelopes is a strong function of both mass and age (Basri et al. 1996; Chabrier et al. 1996; Bildsten et al. 1997). The presence and strength of lithium therefore act as a sensitive chronometer for masses between about 0.06–0.6 $M_\odot$.

Lithium is apparent in 58 stars from the subset of our parent sample for which we obtained spectra (632 out of 2060 stars; see Tables 1 and 3). Line profiles are fit with Gaussian functions to calculate equivalent widths. We estimate uncertainties of about 20% based on multiple measurements of the same targets in our sample. Our low-resolution observations are shown in Figure 5 and are sensitive to the strongest lines, so there are likely to be additional stars with weaker levels of lithium below our detection limits (about 50–200 mÅ) to which we were not sensitive.

Equivalent widths range from ≈100–600 mÅ and span the full range of spectral types from K5 to M5 (middle panel; Figure 4). The diversity of line strengths implies a range of ages for these stars, with the highest equivalent widths corresponding to ages at least as young as TWA (≈10 Myr) based on empirical lithium depletion boundaries for young clusters (e.g., Neuhäuser 1997; Mentuch et al. 2008). For spectral types >K7, all of our stars exhibiting lithium are expected to have ages younger than the Pleaides (≈125 Myr; Stauffer et al. 1998). We note that our lithium stars tend to have high Hα emission-line strengths (top panel; Figure 4) and lower sodium values (lower panel), pointing to higher magnetic activity levels, larger physical radii, and lower surface gravities.

Figure 6 shows the position of our lithium-rich stars in the *Gaia* color–magnitude diagram (CMD) relative to known members of YMGs. The *Gaia* DR2 CMD is constructed by largely adhering to recommendations by Lindegren et al. (2018) with the following additional restrictions: parallaxes >10 mas; parallax S/N > 10; and photometric S/N > 10 in the G, G_B, and G_R bandpasses. Most of the lithium stars lie above the main sequence and are consistent with the isochrones traced out by AB Dor (≈120 Myr); Tuc-Hor, Argus, Carina, and Columba (≈40–50 Myr); β Pic (≈23 Myr); and TWA (≈10 Myr).

4.1.3. Sodium

Like other alkali elements, the relative strength of the Na I doublet at 8183 and 8195 Å is sensitive to atmospheric pressure and surface gravity (e.g., Slesnick et al. 2006). Schlieder et al. (2012a) showed that this doublet can act as a useful tracer of youth for spectral types >M3 because of its prominence relative to the pseudo-continuum at cool temperatures and its stronger dependence on surface gravity at lower masses. We simultaneously fit two Gaussians to these neighboring lines and report the total equivalent width of the pair for each spectrum in Table 1. The bottom panel of Figure 4 shows a general strengthening of the lines at lower temperatures with significant spread for a given spectral type. Beyond M0, stars with lithium tend to lie near the lower envelope of our sodium measurements, in agreement with the expectation of large radii, low surface gravities, and young ages for these objects.

4.2. Visual Binaries

Point sources are identified in our Robo-AO images following the procedure described in Ziegler et al. (2017).

Table 3
Properties of Lithium-rich Stars

2MASS Name	SpT	SpT Reference	RV (km s^{-1})	RV Reference	$\mu_\alpha \cos(\delta)$[a] (mas yr^{-1})	μ_δ[a] (mas yr^{-1})	Distance[a] (pc)	BANYAN Σ Best Hyp.	Literature YMG	Adopted YMG	YMG Reference
J00233468+2014282	M0	TW	−2.2 ± 0.6	Sh17	65.97 ± 0.10	−37.38 ± 0.11	62.89 ± 0.25	Field	β Pic	β Pic	Le09, Ma13, Ma14a, Sh17
J00345120–6154583	K7	TW	11 ± 5	Kr14	88.69 ± 0.04	−52.66 ± 0.04	44.50 ± 0.05	Tuc-Hor	Tuc-Hor	Tuc-Hor	Zu00, Zu01a, To08, Kr14
J00501752+0837341	M5	TW	2.15 ± 2.0	Sh17	68.02 ± 0.26	−35.05 ± 0.13	60.86 ± 0.52	Field	β Pic	β Pic	Sh17
J01001613+1251007	K5	TW	⋯	⋯	47.41 ± 0.08	−31.57 ± 0.06	94.15 ± 0.41	Field	⋯	Field	⋯
J01373940+1835332	K7	TW	0.7 ± 1.9	Sh17	74.76 ± 0.22	−43.35 ± 0.15	52.15 ± 0.28	β Pic	β Pic/Col?	β Pic	Sch10, Ma14b, Sh17
J01540267–4040440	K7	TW	12.7 ± 0.2	Ma14a	48.72 ± 0.03	−15.14 ± 0.03	88.93 ± 0.21	Field	Col	Col	Ma14a
J02490228–1029220	M2	TW	⋯	⋯	44.1 ± 1.9[b]	−21.7 ± 2.3[b]	⋯	Field	β Pic?	β Pic?	Ber15
J03451450+5615353	K7	TW	−9 ± 3	GC18	27.55 ± 0.20	−33.06 ± 0.19	112.64 ± 1.88	Field	⋯	Field	⋯
J03520223+2439479	K7	TW	3.7 ± 0.1	Ng12	31.15 ± 0.93	−41.46 ± 0.87	450 ± 161[c]	Field	Pleiades	Pleiades	St07
J04071148–2918342	M1	TW	21.2 ± 0.3	Ma14a	42.0 ± 1.1[b]	−6.9 ± 1.0[b]	⋯	Col	Col	Col	Ro13, Ma13, Ma14a
J04174964+0011455	K7	TW	19 ± 3	GC18	33.08 ± 0.19	−26.49 ± 0.12	99.72 ± 1.10	Field	⋯	Field	⋯
J04214271–1657543	M1	TW	10 ± 3	GC18	30.9 ± 1.7[b]	−8.0 ± 2.1[b]	⋯	Field	⋯	Field	⋯
J04412079–1947356	K7	TW	⋯	⋯	37.61 ± 1.19	−12.11 ± 1.16	139.81 ± 14.84	Field	⋯	Field	⋯
J04435686+3723033	M2	TW	6.4 ± 0.2	Ma14a	22.87 ± 0.10	−61.84 ± 0.06	71.6 ± 0.26	Field	β Pic	β Pic?	Sch10, Ma14b, Me17, Sh17
J04522204+4006347	M0	TW	⋯	⋯	17.16 ± 0.14	−50.82 ± 0.09	89.1 ± 0.41	Field	⋯	Field	⋯
J04580897+4333010	G/K:	TW	11 ± 8	GC18	22.28 ± 0.17	−55.80 ± 0.13	99.04 ± 1.08	Field	⋯	Field	⋯
J05004928+1527006	K7	TW	18.1 ± 0.9	Wh07	18.13 ± 0.08	−58.83 ± 0.05	53.41 ± 0.12	β Pic	β Pic?	β Pic	Sch12c, Sch12a
J05053647–5755359	K4	TW	⋯	⋯	26.34 ± 0.15	15.83 ± 0.14	94.22 ± 0.67	Field	⋯	Field	⋯
J05182904–3001321	K7	TW	21.0 ± 0.5	El14	37.14 ± 0.08	0.13 ± 0.10	67.01 ± 0.26	Tuc-Hor	Tuc-Hor	Tuc-Hor	To08
J05214684+2400444	G7	Li98	13.1 ± 0.5	Kr17	10.87 ± 0.08	−46.14 ± 0.05	88.27 ± 0.32	118 Tau	118 Tau	118 Tau	Ma16
J05234246+0651581	M0	TW	12 ± 6	GC18	9.75 ± 0.06	−33.46 ± 0.05	96.37 ± 0.36	32 Ori	32 Ori	32 Ori	Bel15
J05363633+2139330	M2	TW	⋯	⋯	10.65 ± 0.19	−41.23 ± 0.14	108.22 ± 1.59	118 Tau	118 Tau, Taurus	118 Tau	Ma16, Kr17
J05374649+0231264	K5	El14	20.8 ± 2.8	GC18	18.28 ± 0.06	−39.52 ± 0.06	68.44 ± 0.19	Field	Col	Col	DaS09, El16
J05500858+0511536	M2	TW	18 ± 4	GC18	17.07 ± 0.07	−42.18 ± 0.06	64.45 ± 0.17	Col	⋯	Col?	TW
J08040534–6316396	M2	TW	⋯	⋯	−17.33 ± 0.05	32.35 ± 0.05	78.10 ± 0.14	Car	Car?	Car?	Ga18c
J08410608–6216063	M0	TW	⋯	⋯	−17.1 ± 1.1[b]	21.8 ± 1.1[b]	⋯	Field	⋯	Field	⋯
J08443188–7846311	M0	TW	17.32 ± 0.11	El14	−30.30 ± 0.06	26.86 ± 0.05	98.18 ± 0.30	η Cha	η Cha	η Cha	Ma99, To08
J09595765–7221472	K7	TW	17.0 ± 0.2	El14	−27.92 ± 0.03	28.95 ± 0.03	83.66 ± 0.13	Field	Car	Car	El15
J10260210–4105537	M2	TW	⋯	⋯	−46.38 ± 0.04	−1.85 ± 0.04	84.88 ± 0.21	Field	TWA, LCC?	TWA	Pe16, Ga17
J11594608–6101132	K4	TW	15 ± 3	GC18	−34.21 ± 0.05	−7.88 ± 0.04	119.45 ± 0.43	LCC	LCC	LCC	Pe16
J12000160–1731308	M4	TW	2 ± 4	GC18	−78.72 ± 0.14	−28.21 ± 0.07	53.12 ± 0.25	Field	⋯	Field	⋯
J12002750–3405371	M5	TW	⋯	⋯	−58.75 ± 0.12	−21.69 ± 0.07	72.79 ± 0.48	TWA	TWA	TWA	Mu15, Ga15b, Ga17
J12003688–6337055	M0	TW	14.3 ± 1.8	GC18	−40.36 ± 0.04	−8.18 ± 0.04	101.2 ± 0.28	LCC	⋯	LCC	TW
J12124890–6230317	K7	TW	⋯	⋯	−41.6 ± 1.4[b]	−4.4 ± 1.8[b]	⋯	LCC	LCC	LCC	So12, El15
J12164593–7753333	M3	TW	14.0 ± 0.2	El14	−39.83 ± 0.07	−9.07 ± 0.07	101.8 ± 0.40	ϵ Cha	ϵ Cha	ϵ Cha	Lo13, Mu13
J12220147–5737565	M2	TW	⋯	⋯	−36.09 ± 0.06	−11.25 ± 0.06	106.45 ± 0.57	LCC	LCC	LCC	Be18
J12264842–5215070	K7	TW	11.6 ± 2.5	GC18	−39.69 ± 0.11	−13.20 ± 0.10	97.18 ± 1.03	LCC	LCC	LCC	Pe16
J12281909–7306346	M0	TW	14.6 ± 1.2	GC18	−36.36 ± 0.31	−7.18 ± 0.32	107.35 ± 2.3	ϵ Cha	⋯	ϵ Cha/LCC	TW
J12383556–5916438	K5	TW	⋯	⋯	−38.01 ± 0.10	−11.17 ± 0.07	100.62 ± 0.77	LCC	LCC	LCC	So12
J12445897–6026409	M1	TW	11.67 ± 0.14	GC18	−32.60 ± 0.44	−9.55 ± 0.54	100.15 ± 3.09	LCC	⋯	LCC	TW
J13343188–4209305	K3	TW	4.3 ± 2.6	GC18	−38.78 ± 0.08	−27.57 ± 0.11	92.81 ± 0.42	UCL	LCC?	UCL/LCC	So12, De15
J13390189–2141278	M4	TW	2.8 ± 1.6	Ma14a	−41.98 ± 0.12	−26.91 ± 0.13	83.81 ± 0.54	Field	⋯	Field	⋯
J13493313–6818291	M3	TW	⋯	⋯	−31.05 ± 0.21	−19.71 ± 0.23	99.76 ± 1.51	LCC	Arg?	LCC	Ma13, TW

Table 3
(Continued)

2MASS Name	SpT	SpT Reference	RV (km s^{-1})	RV Reference	$\mu_\alpha \cos(\delta)$[a] (mas yr^{-1})	μ_δ[a] (mas yr^{-1})	Distance[a] (pc)	BANYAN Σ Best Hyp.	Literature YMG	Adopted YMG	YMG Reference
J15093920–1332119	M5	TW	⋯	⋯	−53.01 ± 0.17	−49.11 ± 0.12	52.65 ± 0.23	Field	⋯	Field	⋯
J15202415–3037317	M0	TW	⋯	⋯	−27.78 ± 0.10	−33.12 ± 0.07	123.92 ± 0.93	UCL	UCL	UCL	Pe16
J15354856–2958551	M4	TW	⋯	⋯	−32.7 ± 1.7[b]	−38.1 ± 1.7[b]	⋯	Field	USco-B	UCL?	Ko00, TW
J15443518+0423075	M2	TW	−22 ± 5	GC18	−25.42 ± 0.06	−27.19 ± 0.05	91.96 ± 0.28	Field	⋯	Field	⋯
J15451903–4431361	M3	TW	⋯	⋯	−20.41 ± 1.16	−30.90 ± 1.10	89.33 ± 3.68	UCL	⋯	UCL?	TW
J15594951–3628279	K5	TW	−0.3 ± 1.2	So12	−28.47 ± 0.10	−43.12 ± 0.06	86.62 ± 0.42	UCL	UCL	UCL	So12, Pe16
J16082845–0607345	M4	TW	⋯	⋯	−18.77 ± 0.16	−26.39 ± 0.08	86.55 ± 0.53	Field	⋯	Field	⋯
J16430128–1754274	M1	TW	−9.3 ± 0.4	Ma14a	−29.13 ± 0.10	−52.03 ± 0.05	71.05 ± 0.26	Field	β Pic	Field	Ki10, Bi14, Sh17
J16455062+0343014	M2	TW	−21.7 ± 1.8	GC18	−37.67 ± 0.08	−105.38 ± 0.07	44.89 ± 0.08	AB Dor	AB Dor?	AB Dor?	Sch12a, Sch12b, Bi15b
J16521087–3359333	M0	TW	⋯	⋯	−20.3 ± 2.0[b]	−42.7 ± 1.2[b]	⋯	UCL	UCL	UCL	So12
J17213497–2152283	M4	TW	⋯	⋯	−11.82 ± 0.15	−32.99 ± 0.09	101.04 ± 0.73	UCL	⋯	Sco-Cen?	TW
J17513421–4854558	M2	TW	⋯	⋯	2.14 ± 0.47	−66.85 ± 0.41	66.46 ± 1.17	β Pic	USco, β Pic	β Pic	So12, Ga18c
J17520173–2357571	M2	TW	⋯	⋯	0.22 ± 0.09	−52.24 ± 0.07	63.52 ± 0.20	Field	⋯	Field	⋯
J17563029–2448128	M2	TW	⋯	⋯	−6.58 ± 0.10	−37.02 ± 0.08	95.60 ± 0.58	Field	⋯	Field	⋯
J23093711–0225551	K4	To06	−12.7 ± 0.4	GC18	60.84 ± 0.11	−45.96 ± 0.11	52.60 ± 0.41	Field	Car	Field?	El15, El16

Notes.
[a] Proper motions and parallactic distance from *Gaia* DR2, unless otherwise noted.
[b] Proper motion from UCAC4 (Zacharias et al. 2013).
[c] Large excess noise parameter in *Gaia* DR2, implying the astrometric solution may not be reliable.

References. Be18—Goldman et al. (2018), Bel15—Bell et al. (2015), Ber15—Bergfors et al. (2016), Bi14—Binks & Jeffries (2014), Bi15b—Binks & Jeffries (2015), DaS09—da Silva et al. (2009), De15—Desidera et al. (2015), El14—Elliott et al. (2014), El15—Elliott et al. (2015), El16—Elliott et al. (2016), Ga15b—Gagné et al. (2015), Ga17—Gagné et al. (2017), Ga18c—Gagné & Faherty (2018), GC18—Gaia Collaboration et al. (2018) Ki10—Kiss et al. (2010), Ko00—Köhler et al. (2000), Kr14—Kraus et al. (2014), Kr17—Kraus et al. (2017), Le09—Lépine & Simon (2009), Li98—Li & Hu (1998), Lo13—López Martí et al. (2013), Ma99— Mamajek et al. (1999), Ma16—Mamajek (2016a), Ma13—Malo et al. (2013), Ma14a—Malo et al. (2014a), Ma14b—Malo et al. (2014b), Me17—Messina et al. (2017), Mu13—Murphy et al. (2013), Mu15—Murphy et al. (2015), Ng12—Nguyen et al. (2012), Pe16—Pecaut & Mamajek (2016), Ro13—Rodriguez et al. (2013), Sch10—Schlieder et al. (2010), Sch12a—Schlieder et al. (2012b), Sch12b—Schlieder et al. (2012c), Sch12c—Schlieder et al. (2012a), Sh17—Shkolnik et al. (2017), So12—Song et al. (2012), St07—Stauffer et al. (2007), To06—Torres et al. (2006), To08—Torres et al. (2008), TW—This work, Wh07—White et al. (2007), Zu00—Zuckerman & Webb (2000), Zu01a—Zuckerman et al. (2001b).

(This table is available in its entirety in machine-readable form.)

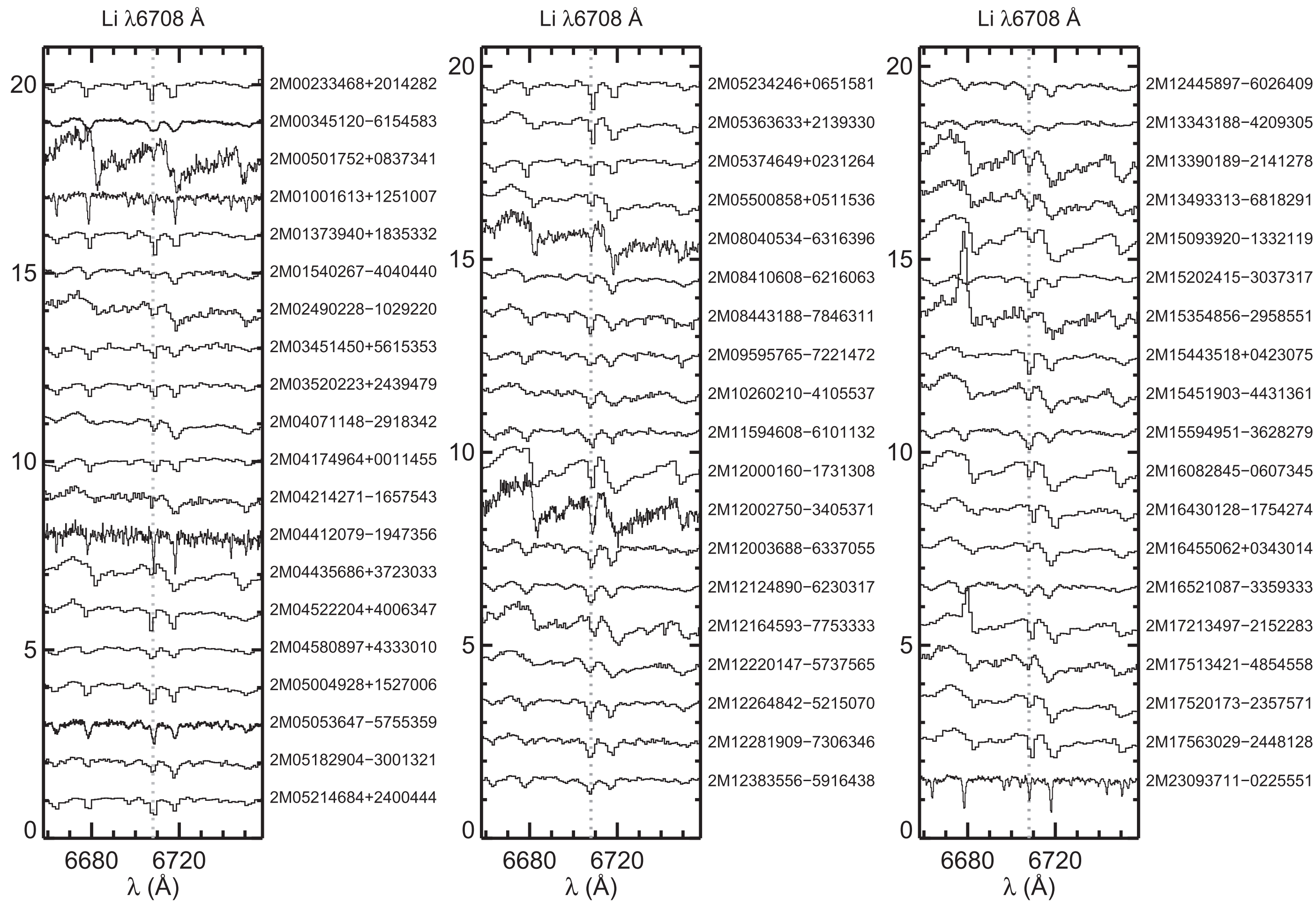

Figure 5. Spectra of 58 lithium-rich stars from the subset of activity-selected targets for which we obtained follow-up spectroscopy. The observations were taken with several spectrographs and modes spanning a range of resolving powers from $R \approx 1300$–5900 (details can be found in Table 1). The Li I λ6708 line is marked with a gray dotted line.

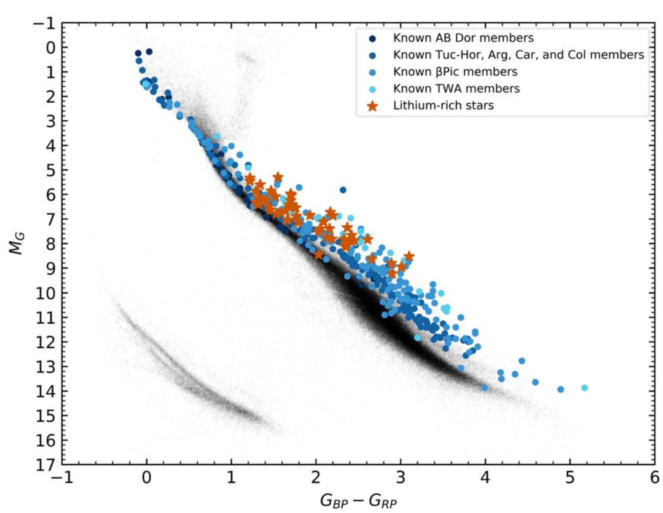

Figure 6. Positions of lithium-rich stars (red stars) in the *Gaia* color–magnitude diagram relative to known moving group members from Malo et al. (2013). The *Gaia* color–magnitude diagram shows stars within 100 pc with spurious entries removed following Lindegren et al. (2018).

Each image is inspected visually and through an automated source-finding algorithm. We focus on a 4″ radius surrounding each star where our AO observations are most advantageous compared to all-sky seeing-limited surveys. Altogether, point sources are found near 239 stars with optical contrasts peaking at $\Delta\text{mag} \approx 0.5$ and reaching $\Delta\text{mag} \approx 7$ for the faintest objects identified (Figures 7–10). Relative contrasts are measured using aperture photometry at wide separations and processed images of the companion after PSF subtraction at close separations. Uncertainties in astrometry and contrast are estimated based on systematic errors caused by blending and due to maximum orientation changes during the observing period, which we estimate to be $\pm 1\overset{\circ}{.}5$ using calibration fields. Contrasts, separations, position angles, and estimated uncertainties for all point sources can be found in Table 4. Note that targets reported in our complete list of observations in Table 2 that do not have nearby point sources listed in Table 4 imply that they are single, at least to within our sensitivity limits.

In Table 5, we compare the observed and expected astrometry for candidate binary companions with multi-epoch imaging to test whether they are background stars or physically bound systems. χ^2 values for the common proper motion (χ^2_{CPM}) and background (χ^2_{BG}) hypotheses are calculated as follows:

$$\chi^2_{\text{CPM}} = \sum_{i=1}^{N-1}\left(\frac{(\theta_{\text{meas},i} - \theta_{\text{ref},i})^2}{\sigma^2_{\theta,\text{meas},i} + \sigma^2_{\theta,\text{ref},i}} + \frac{(\rho_{\text{meas},i} - \rho_{\text{ref},i})^2}{\sigma^2_{\rho,\text{meas},i} + \sigma^2_{\rho,\text{ref},i}}\right),$$

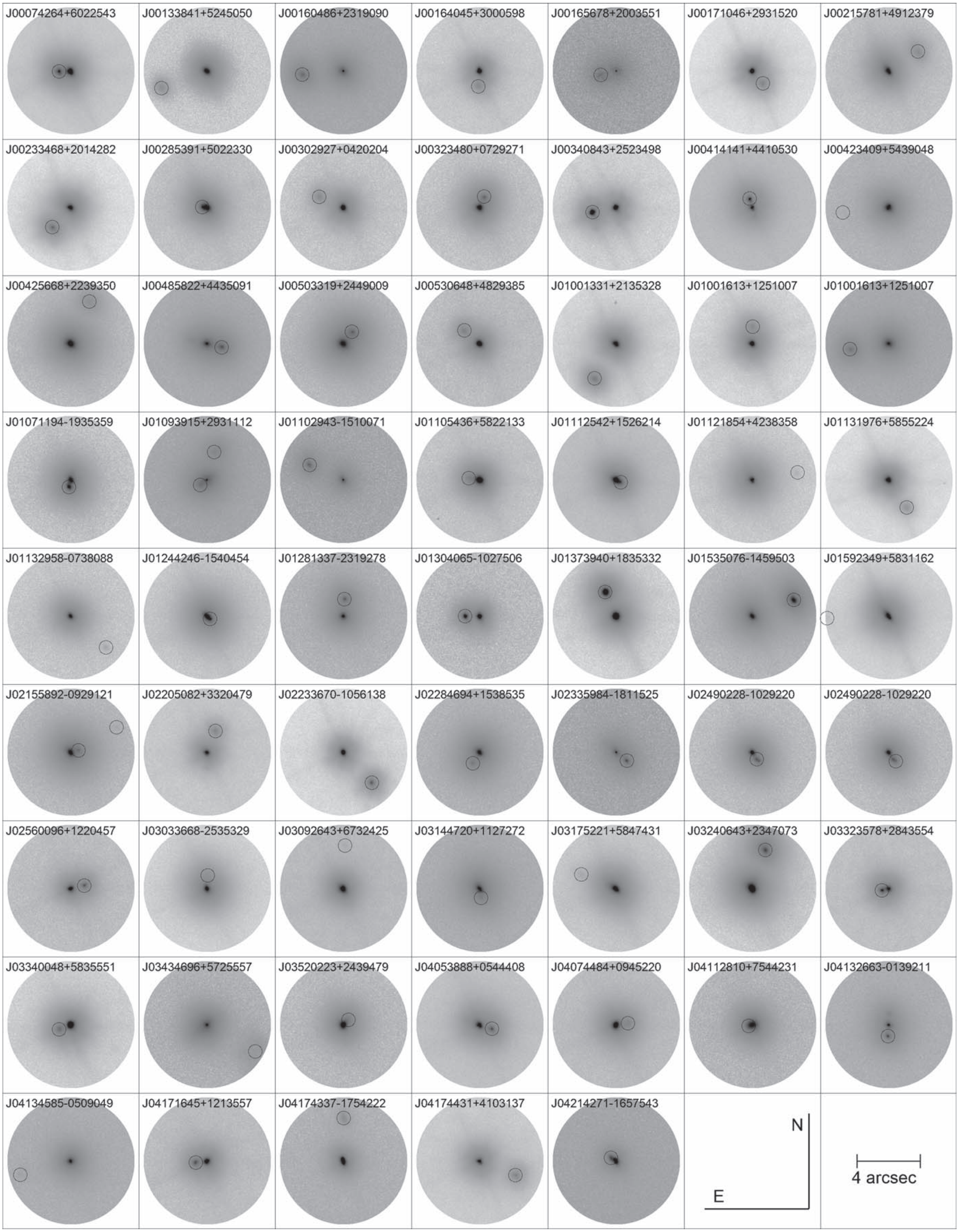

Figure 7. Point sources identified in our Robo-AO observations for R.A. between 00 and 04 hr. Circles mark the locations of point sources. The field of view of each image is $8'' \times 8''$. The sky orientation is denoted at the bottom right of the figure.

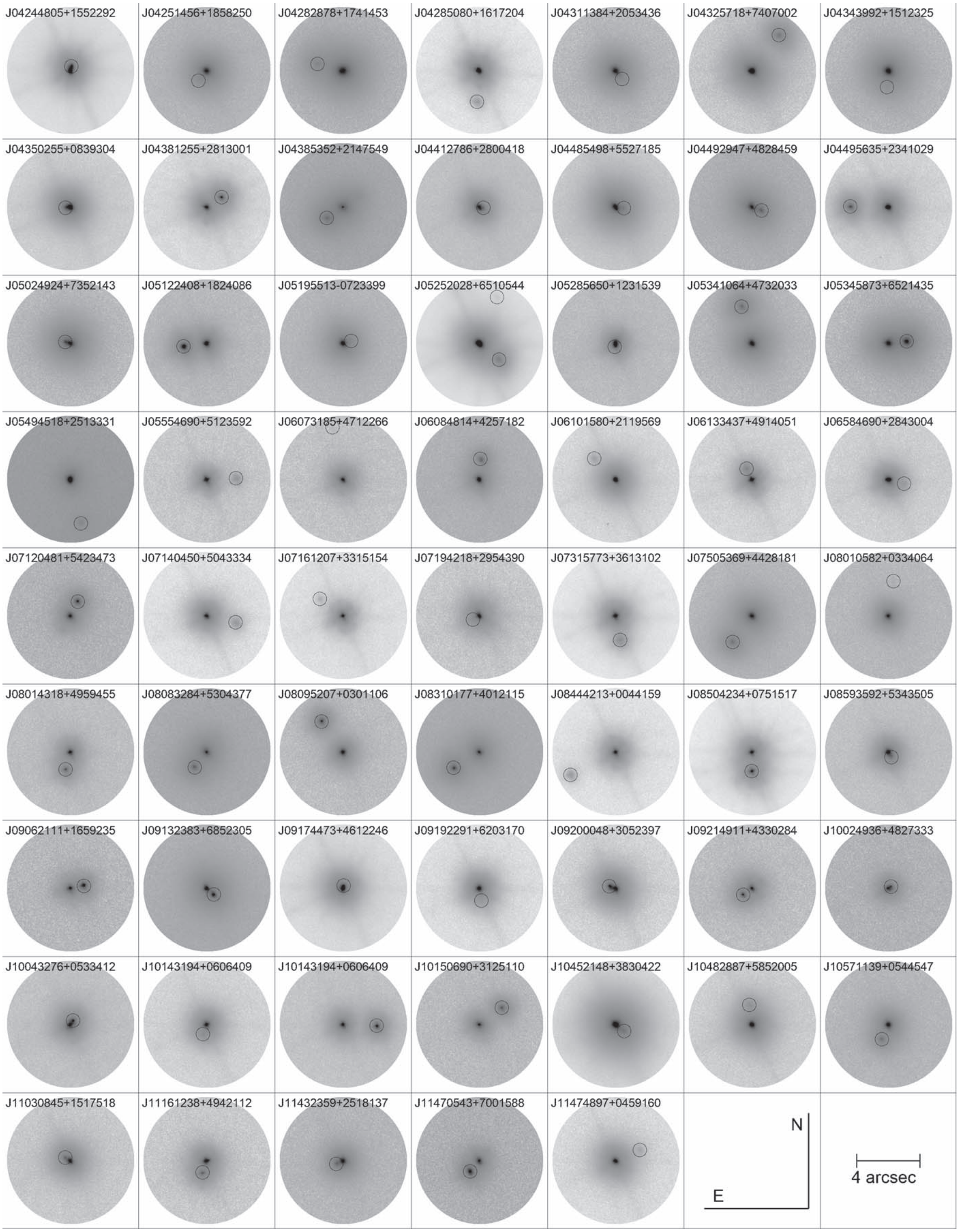

Figure 8. Same as Figure 7 but for R.A.s between 04 and 11 hr.

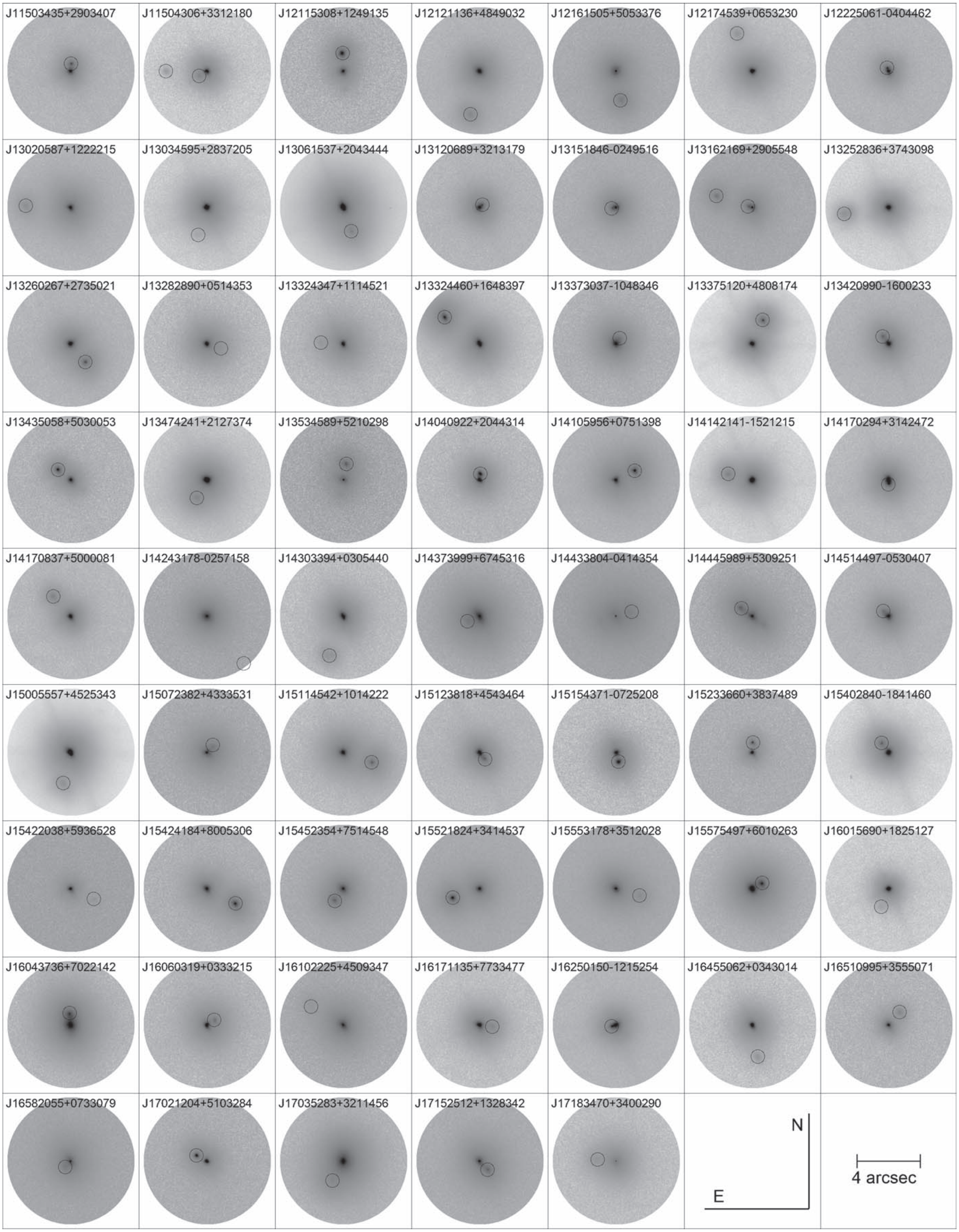

Figure 9. Same as Figure 7 but for R.A.s between 11 and 17 hr.

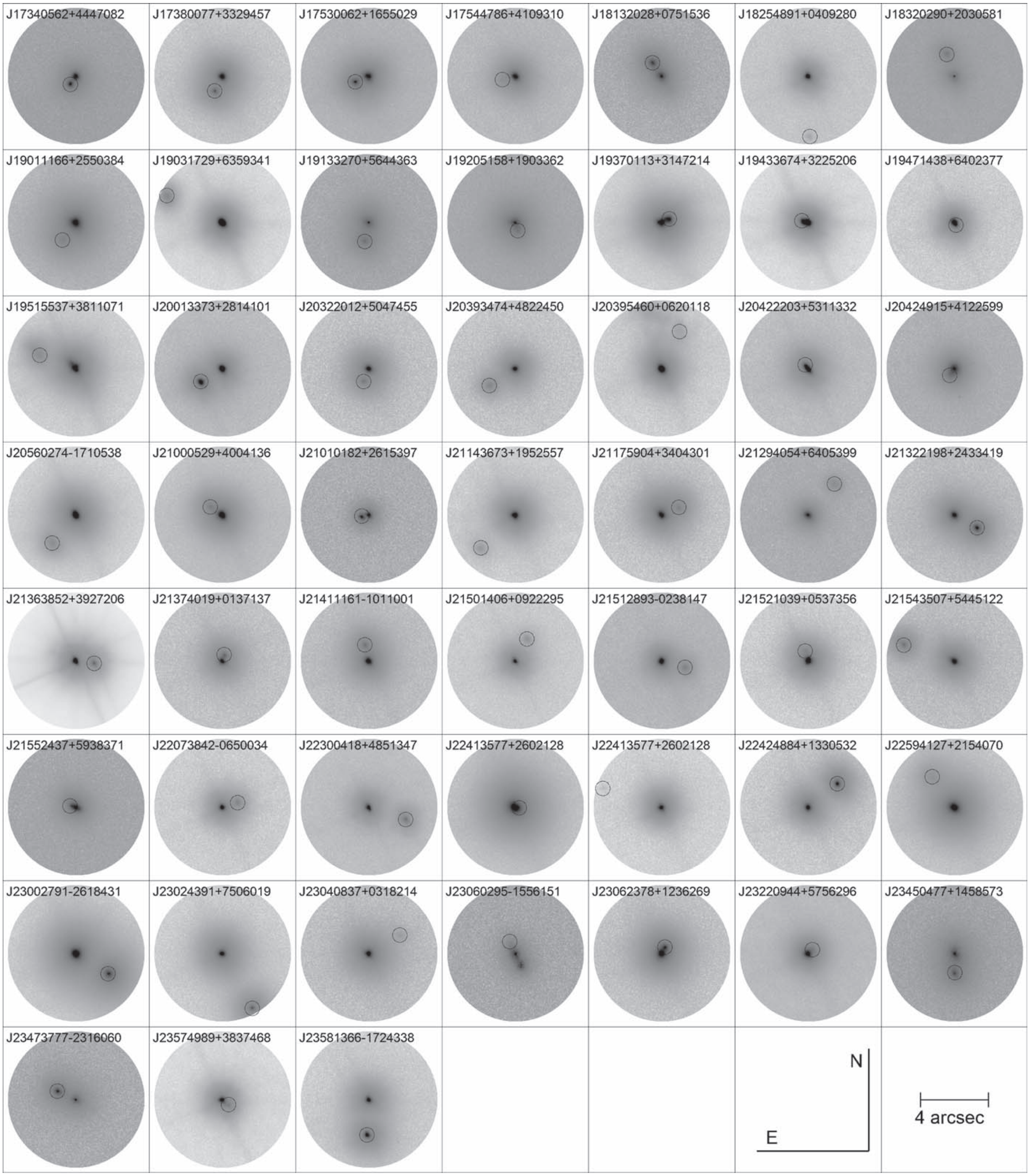

Figure 10. Same as Figure 7 but for R.A.s between 17 and 00 hr.

$$\chi^2_{\rm BG} = \sum_{i=1}^{N-1}\left(\frac{(\theta_{{\rm meas},i} - \theta_{{\rm pred},i})^2}{\sigma^2_{\theta,{\rm meas},i} + \sigma^2_{\theta,{\rm pred},i}} + \frac{(\rho_{{\rm meas},i} - \rho_{{\rm pred},i})^2}{\sigma^2_{\rho,{\rm meas},i} + \sigma^2_{\rho,{\rm pred},i}}\right).$$

Here, $\theta_{{\rm meas},i}$, $\rho_{{\rm meas},i}$, $\sigma_{\theta,{\rm meas},i}$, and $\sigma_{\rho,{\rm meas},i}$ are the measured P.A., separation, and their respective uncertainties for epoch i of N total epochs; $\theta_{{\rm ref},i}$, $\rho_{{\rm ref},i}$, $\sigma_{\theta,{\rm ref},i}$, and $\sigma_{\rho,{\rm ref},i}$ are the same for the reference epoch (here taken to be our first observation of the system); and $\theta_{{\rm pred},i}$, $\rho_{{\rm pred},i}$, $\sigma_{\theta,{\rm pred},i}$, and $\sigma_{\rho,{\rm pred},i}$ are the predicted relative astrometry of a stationary background source based on the distance, proper motion, and sky position of the target (Table 6).

The Bayesian Information Criterion (BIC; Schwarz 1978) is used to assess the significance of evidence for or against the

Table 4
Robo-AO Point Source Detections

2MASS ID	UT Date (Y-M-D)	Filter	Candidate Name	Δmag	Sep (″)	P.A. (°)	Significance (σ)	Performance Metric[a]
J00074264+6022543	2014 Nov 8	i'	CC1	0.30 ± 0.05	0.86 ± 0.03	94 ± 2	12.5	H
J00133841+5245050	2014 Aug 26	i'	CC1	2.76 ± 0.03	3.13 ± 0.03	110 ± 3	11.5	H
J00133841+5245050	2014 Nov 6	i'	CC1	2.39 ± 0.05	3.16 ± 0.04	109 ± 2	7.2	M
J00133841+5245050	2014 Nov 6	i'	CC1	2.74 ± 0.02	3.16 ± 0.04	109 ± 3	6.4	H
J00133841+5245050	2014 Nov 6	i'	CC2	3.41 ± 0.04	0.86 ± 0.03	94 ± 2	5.9	M
J00160486+2319090	2014 Nov 6	i'	CC1	0.41 ± 0.05	2.66 ± 0.05	94 ± 2	9.6	M
J00164045+3000598	2014 Aug 24	i'	CC1	2.47 ± 0.03	0.98 ± 0.03	174 ± 1	12.4	H
J00165678+2003551	2014 Nov 6	i'	CC1	0.21 ± 0.03	1.03 ± 0.05	102 ± 3	4.2	H
J00171046+2931520	2013 Oct 23	i'	CC1	2.07 ± 0.05	1.02 ± 0.02	218 ± 1	10.5	H
J00171046+2931520	2014 Aug 28	i'	CC1	2.03 ± 0.04	1.03 ± 0.04	221 ± 6	12.7	H

Note.
[a] Image performance metrics assessed from the PSF core size. These are divided into three groups: high performance ("H"), medium performance ("M"), and low performance ("L"). Typical contrasts for each group are described in detail in Section 3.4.

(This table is available in its entirety in machine-readable form.)

background and comoving models. It is constructed to reward better fits but penalize more complex models as follows:

$$\mathrm{BIC} \quad = \quad \chi^2 + k \ln n,$$

where k is the number of free parameters in the model and n is the number of epochs. Lower BIC values are preferred. Differenced BIC values ($\Delta\mathrm{BIC} = \mathrm{BIC}_{\mathrm{BG}}–\mathrm{BIC}_{\mathrm{CPM}}$) for both bound and unbound scenarios are listed in Table 5. Following Kass & Raftery (1995), ΔBIC values between 0 and 3 are interpreted as modest evidence in favor of common proper motion, ΔBIC values greater than 3 suggest strong evidence for common proper motion, ΔBIC values between 0 and −3 point to modest evidence in favor of the background model, and ΔBIC values less than −3 imply strong evidence for the background model.

A total of 252 sources are detected within 4″ of 239 stars. A single epoch was acquired for most candidate companions so some sources may be background stars, but the vast majority are expected to be physical binaries based on the low number density of comparably bright stars. We carried out a literature search primarily consulting the Washington Double Star Catalog (Mason et al. 2001) and identified 88 previously known binaries—most of which have undergone significant orbital motion since their discovery—while the rest appear to be new.

4.3. YMG Members

Among the 58 lithium-rich stars in our sample, 35 are previously known or suspected members of YMGs or nearby star-forming regions (Table 3). Similarly, 51 out of the 238 visual binaries have been identified as known or candidate YMG members in the literature (Table 6). We used the BANYAN-Σ tool from Gagné et al. (2018b) to search for additional YMG members in our our lithium-rich stars and active binary samples. BANYAN-Σ is a Bayesian classifier that uses kinematic information to determine an object's membership probability for YMGs within 150 pc. Compared to previous versions of BANYAN (Malo et al. 2013; Gagné et al. 2014), this updated package uses a refined model of the galactic disk together with spatial and kinematic constraints for 27 associations with ages $\lesssim$800 Myr, including nearby star-forming regions and intermediate-age open clusters.

Results from the BANYAN analysis using default parameters for association locations and space motions are listed in Tables 3 and 6. When available, radial velocities from the literature have been used for the lithium-rich sample. We do not make use of an instantaneous radial velocity measurement for the active binaries since long-baseline monitoring is needed to robustly measure the pair's systemic velocity. The best hypothesis refers to the most probable kinematic and spatial model, including the field. Results from BANYAN broadly agree with previous assessments, but in many cases either identifies the field as the most likely hypothesis or disagrees on the most likely moving group. Altogether an additional seven and ten systems are identified as new candidate moving group members from the lithium-rich and active binary samples, respectively.

5. Notes on Individual Objects

Below we comment on new candidate YMG members, noteworthy individual systems with unusually high Hα emission, and objects with discrepancies between BANYAN-Σ and literature YMG assessments from Tables 3 and 6. Our final adopted membership status takes into account lithium line strength, *UVW* kinematics, spatial position, sky position, and CMD position when possible.

2MASS J00233468+2014282—Lépine & Simon (2009) first identified this star as a member of β Pic, which has been bolstered by several additional studies (Malo et al. 2013, 2014a; Shkolnik et al. 2017). However, the best hypothesis from BANYAN-Σ is the field population. We measure modest lithium absorption (EW ≈ 260 mÅ), weak Hα emission (EW = −1 Å), and a spectral type of M0 from our Mayall spectrum, in close agreement with previous measurements. The observed lithium strength is typical of β Pic members of this spectral type. This target is identified as a 1$''$.7 binary in the Washington Double Star catalog; we easily recovered this companion with our Robo-AO observations. Using the measured radial velocity (RV) of -2.2 ± 0.6 km s^{-1} from Shkolnik et al. (2017) together with *Gaia* DR2 astrometry, the space velocities of this system are $U = -11.81 \pm 0.19$ km s^{-1}, $V = -17.4 \pm 0.4$ km s^{-1}, and $W = -8.8 \pm 0.4$ km s^{-1}. This

Table 5
Binary Common Proper Motion Tests

2MASS Name	$N_{\rm epochs}$	Δt (yr)	Cand. Comp.	χ^2_ν (BG)	χ^2_ν (CPM)	ν	BIC (BG)	BIC (CPM)	ΔBIC	Comp?[a]	Known Binary?	Binary Reference
J00074264+6022543	1	···	CC1	···	···	0	···	···	···	SE	Y	Ja14b, Bo15b
J00133841+5245050	3	0.197	CC1	0.352	0.426	2	6.20	6.35	−0.148	BG?	N	···
J00133841+5245050	1	···	CC2	···	···	0	···	···	···	SE	N	···
J00160486+2319090	1	···	CC1	···	···	0	···	···	···	SE	N	···
J00164045+3000598	1	···	CC1	···	···	0	···	···	···	SE	N	···
J00165678+2003551	1	···	CC1	···	···	0	···	···	···	SE	N	···
J00171046+2931520	2	0.847	CC1	0.307	0.293	1	3.77	3.76	0.0133	CPM?	N	···
J00215781+4912379	4	0.828	CC1	14.1	0.795	3	49.2	9.32	39.9	CPM	Y	Bo15b
J00215781+4912379	1	···	CC2	···	···	0	···	···	···	SE	N	···
J00233468+2014282	1	···	CC1	···	···	0	···	···	···	SE	Y	WDS
J00285391+5022330	1	···	CC1	···	···	0	···	···	···	SE	Y	Dae07
J00302927+0420204	1	···	CC1	···	···	0	···	···	···	SE	N	···
J00323480+0729271	2	0.828	CC1	5.51	0.481	1	8.98	3.95	5.03	CPM	Y	Mc01
J00340843+2523498	2	0.836	CC1	2.49	0.0799	1	5.95	3.55	2.41	CPM?	Y	WDS
J00414141+4410530	2	1.04	CC1	14.9	4.26	1	18.4	7.73	10.6	CPM	Y	Ja12
J00423409+5439048	3	0.208	CC1	0.285	0.357	2	6.06	6.21	−0.144	BG?	N	···
J00425668+2239350	1	···	CC1	···	···	0	···	···	···	SE	Y	WDS
J00485822+4435091	2	1.04	CC1	16.1	2.46	1	19.5	5.93	13.6	CPM	Y	Mc01
J00503319+2449009	2	1.04	CC1	18.8	1.78	1	22.3	5.25	17.0	CPM	Y	WDS, Ja12
J00530648+4829385	1	···	CC1	···	···	0	···	···	···	SE	N	···
J01001331+2135328	1	···	CC1	···	···	0	···	···	···	SE	N	···
J01001613+1251007	2	0.830	CC1	0.670	0.156	1	4.14	3.62	0.515	CPM?	N	···
J01034013+4051288	1	···	CC1	···	···	0	···	···	···	SE	N	···
J01071194–1935359	1	···	CC1	···	···	0	···	···	···	SE	N	···
J01093915+2931112	1	···	CC1	···	···	0	···	···	···	SE	N	···
J01102943–1510071	1	···	CC1	···	···	0	···	···	···	SE	Y	WDS
J01105436+5822133	1	···	CC1	···	···	0	···	···	···	SE	N	···
J01112542+1526214	1	···	CC1	···	···	0	···	···	···	SE	Y	Beu04
J01121854+4238358	3	0.833	CC1	2.53	0.0478	2	10.6	5.59	4.97	CPM	N	···
J01121854+4238358	1	···	CC2	···	···	0	···	···	···	SE	N	···
J01131976+5855224	2	0.839	CC1	3.17	0.0800	1	6.63	3.55	3.09	CPM	N	···
J01132958–0738088	1	···	CC1	···	···	0	···	···	···	SE	Y	Ja12
J01244246–1540454	1	···	CC1	···	···	0	···	···	···	SE	N	···
J01281337–2319278	1	···	CC1	···	···	0	···	···	···	SE	N	···
J01304065–1027506	1	···	CC1	···	···	0	···	···	···	SE	N	···
J01373940+1835332	2	0.830	CC1	0.703	0.106	1	4.17	3.57	0.597	CPM?	Y	WDS
J01535076–1459503	1	···	CC1	···	···	0	···	···	···	SE	Y	Ber10
J01592349+5831162	5	1.04	CC1	0.414	49.5	4	9.70	206	−196	BG	N	···
J01592349+5831162	1	···	CC2	···	···	0	···	···	···	SE	N	···
J02155892–0929121	1	···	CC1	···	···	0	···	···	···	SE	Y	Ber10, Bo15a
J02155892–0929121	1	···	CC2	···	···	0	···	···	···	SE	Y	Ber10, Bo15a
J02205082+3320479	2	0.830	CC1	8.19	0.200	1	11.7	3.67	7.99	CPM	N	···
J02233670–1056138	1	···	CC1	···	···	0	···	···	···	SE	Y	WDS
J02284694+1538535	1	···	CC1	···	···	0	···	···	···	SE	N	···
J02335984–1811525	1	···	CC1	···	···	0	···	···	···	SE	Y	Ber10
J02490228–1029220	2	···	CC1	26.8	26.1	1	30.2	29.6	0.659	CPM?	Y	Ber10
J02560096+1220457	1	···	CC1	···	···	0	···	···	···	SE	N	···

Table 5
(Continued)

2MASS Name	N_{epochs}	Δt (yr)	Cand. Comp.	χ^2_ν (BG)	χ^2_ν (CPM)	ν	BIC (BG)	BIC (CPM)	ΔBIC	Comp?[a]	Known Binary?	Binary Reference
J03033668–2535329	1	…	CC1	…	…	0	…	…	…	SE	Y	Ber10
J03092643+6732425	1	…	CC1	…	…	0	…	…	…	SE	N	…
J03144720+1127272	2	0.214	CC1	6.94	7.33	1	10.4	10.8	−0.383	BG?	N	…
J03175221+5847431	3	0.828	CC1	2.14	0.114	2	9.77	5.72	4.05	CPM	N	…
J03240643+2347073	4	1.05	CC1	7.14	2.50	3	28.3	14.4	13.9	CPM	Y	WDS
J03323578+2843554	1	…	CC1	…	…	0	…	…	…	SE	Y	Ja12
J03340048+5835551	1	…	CC1	…	…	0	…	…	…	SE	N	…
J03434696+5725557	1	…	CC1	…	…	0	…	…	…	SE	N	…
J03520223+2439479	1	…	CC1	…	…	0	…	…	…	SE	Y	WDS
J04053888+0544408	2	0.828	CC1	5.53	0.692	1	9.00	4.16	4.84	CPM	Y	Mc01
J04074484+0945220	1	…	CC1	…	…	0	…	…	…	SE	N	…
J04112810+7544231	1	…	CC1	…	…	0	…	…	…	SE	N	…
J04132663–0139211	1	…	CC1	…	…	0	…	…	…	SE	Y	Mc01
J04134585–0509049	1	…	CC1	…	…	0	…	…	…	SE	Y	Bo15b
J04171645+1213557	2	0.830	CC1	4.96	2.00	1	8.43	5.47	2.96	CPM?	N	…
J04174337–1754222	1	…	CC1	…	…	0	…	…	…	SE	N	…
J04174431+4103137	2	0.844	CC1	2.29	1.17	1	5.76	4.64	1.11	CPM?	N	…
J04214271–1657543	1	…	CC1	…	…	0	…	…	…	SE	N	…
J04244805+1552292	2	1.04	CC1	25.9	0.940	1	29.3	4.41	24.9	CPM	Y	WDS
J04251456+1858250	1	…	CC1	…	…	0	…	…	…	SE	N	…
J04282878+1741453	2	1.04	CC1	3.71	0.109	1	7.17	3.57	3.60	CPM	Y	Gu05
J04285080+1617204	3	0.830	CC1	0.643	0.281	2	6.78	6.06	0.724	CPM?	N	…
J04285080+1617204	1	…	CC2	…	…	0	…	…	…	SE	N	…
J04311384+2053436	1	…	CC1	…	…	0	…	…	…	SE	N	…
J04325718+7407002	1	…	CC1	…	…	0	…	…	…	SE	N	…
J04343992+1512325	1	…	CC1	…	…	0	…	…	…	SE	N	…
J04350255+0839304	1	…	CC1	…	…	0	…	…	…	SE	N	…
J04381255+2813001	2	1.04	CC1	53.7	0.00	1	57.2	3.47	53.7	CPM	Y	Beu04
J04385352+2147549	1	…	CC1	…	…	0	…	…	…	SE	Y	Ja14b
J04412780+1404340	1	…	CC1	…	…	0	…	…	…	SE	N	…
J04485498+5527185	1	…	CC1	…	…	0	…	…	…	SE	N	…
J04492947+4828459	2	1.05	CC1	32.4	1.29	1	35.8	4.76	31.1	CPM	Y	Ja14b
J04495635+2341029	2	0.844	CC1	2.28	0.860	1	5.74	4.33	1.42	CPM?	N	…
J05024924+7352143	1	…	CC1	…	…	0	…	…	…	SE	Y	Ja12
J05122408+1824086	1	…	CC1	…	…	0	…	…	…	SE	N	…
J05195513–0723399	1	…	CC1	…	…	0	…	…	…	SE	Y	Ja12
J05252028+6510544	1	…	CC1	…	…	0	…	…	…	SE	Y	WDS
J05285650+1231539	1	…	CC1	…	…	0	…	…	…	SE	N	…
J05341064+4732033	3	1.38	CC1	2.00	3.17	2	9.49	11.8	−2.34	BG?	N	…
J05345873+6521435	1	…	CC1	…	…	0	…	…	…	SE	N	…
J05494518+2513331	2	0.839	CC1	7.03	4.20	1	10.5	7.67	2.83	CPM?	N	…
J05554690+5123592	2	0.335	CC1	0.167	0.118	1	3.63	3.58	0.0490	CPM?	N	…
J06073185+4712266	1	…	CC1	…	…	0	…	…	…	SE	N	…
J06084814+4257182	4	1.22	CC1	23.6	2.39	3	77.7	14.1	63.6	CPM	N	…
J06101580+2119569	4	0.852	CC1	2.71	2.28	3	15.1	13.8	1.31	CPM?	N	…
J06101580+2119569	1	…	CC2	…	…	0	…	…	…	SE	N	…
J06133437+4914051	3	1.38	CC1	1.42	0.198	2	8.33	5.89	2.44	CPM?	N	…

Table 5
(Continued)

2MASS Name	N_{epochs}	Δt (yr)	Cand. Comp.	χ^2_ν (BG)	χ^2_ν (CPM)	ν	BIC (BG)	BIC (CPM)	ΔBIC	Comp?[a]	Known Binary?	Binary Reference
J06462622+0521150	1	…	CC1	…	…	0	…	…	…	SE	N	…
J06584690+2843004	6	0.953	CC1	0.507	1.44	5	11.5	16.1	−4.65	BG	N	…
J07120481+5423473	3	0.953	CC1	4.96	2.04	2	15.4	9.57	5.84	CPM	N	…
J07140450+5043334	8	0.953	CC1	9.41	0.528	7	76.3	14.1	62.2	CPM	N	…
J07140450+5043334	1	…	CC2	…	…	0	…	…	…	SE	N	…
J07161207+3315154	3	0.510	CC1	7.60	0.105	2	20.7	5.70	15.0	CPM	N	…
J07194218+2954390	1	…	CC1	…	…	0	…	…	…	SE	N	…
J07315773+3613102	2	1.22	CC1	55.7	0.281	1	59.2	3.75	55.4	CPM	Y	Beu04
J07505369+4428181	3	1.23	CC1	12.3	0.359	2	30.1	6.21	23.9	CPM	Y	Ja12
J08010582+0334064	1	…	CC1	…	…	0	…	…	…	SE	N	…
J08014318+4959455	4	1.23	CC1	4.64	0.697	3	20.8	9.02	11.8	CPM	N	…
J08083284+5304377	3	0.953	CC1	1.33	0.547	2	8.16	6.59	1.57	CPM?	N	…
J08095207+0301106	2	0.321	CC1	1.03	0.400	1	4.50	3.87	0.634	CPM?	N	…
J08310177+4012115	3	1.37	CC1	4.16	0.219	2	13.8	5.93	7.89	CPM	Y	WDS
J08444213+0044159	2	0.321	CC1	1.82	0.00	1	5.29	3.47	1.82	CPM?	N	…
J08504234+0751517	3	0.324	CC1	2.84	0.557	2	11.2	6.61	4.57	CPM	Y	WDS
J08593592+5343505	1	…	CC1	…	…	0	…	…	…	SE	N	…
J09062111+1659235	1	…	CC1	…	…	0	…	…	…	SE	Y	Sc98
J09132383+6852305	2	0.321	CC1	8.08	0.811	1	11.5	4.28	7.27	CPM	N	…
J09174473+4612246	1	…	CC1	…	…	0	…	…	…	SE	Y	Ja12
J09192291+6203170	1	…	CC1	…	…	0	…	…	…	SE	N	…
J09200048+3052397	3	0.953	CC1	3.12	1.71	2	11.7	8.91	2.83	CPM?	N	…
J09214911+4330284	2	0.953	CC1	60.2	0.347	1	63.7	3.81	59.9	CPM	Y	La08
J10024936+4827333	1	…	CC1	…	…	0	…	…	…	SE	N	…
J10043276+0533412	2	0.953	CC1	16.0	0.650	1	19.5	4.12	15.3	CPM	N	…
J10143153+0213174	1	…	CC1	…	…	0	…	…	…	SE	N	…
J10143194+0606409	2	0.953	CC1	22.6	0.692	1	26.0	4.16	21.9	CPM	Y	WDS
J10150690+3125110	3	1.20	CC1	9.44	0.495	2	24.4	6.48	17.9	CPM	N	…
J10452148+3830422	1	…	CC1	…	…	0	…	…	…	SE	Y	WDS
J10482887+5852005	5	1.20	CC1	0.273	8.18	4	9.14	40.8	−31.6	BG	N	…
J10482887+5852005	1	…	CC2	…	…	0	…	…	…	SE	N	…
J10571139+0544547	4	1.20	CC1	3.52	0.555	3	17.5	8.60	8.89	CPM	Y	Bo15b
J11030845+1517518	3	1.20	CC1	62.7	1.54	2	131.	8.57	122.	CPM	N	…
J11161238+4942112	3	1.20	CC1	1.96	0.651	2	9.41	6.79	2.62	CPM?	N	…
J11432359+2518137	2	0.956	CC1	20.8	0.222	1	24.2	3.69	20.5	CPM	N	…
J11470543+7001588	1	…	CC1	…	…	0	…	…	…	SE	N	…
J11474897+0459160	6	1.20	CC1	2.77	0.367	5	22.8	10.8	12.0	CPM	N	…
J11503435+2903407	3	1.20	CC1	8500	3.86	2	17000	13.2	17000	CPM	N	…
J11504306+3312180	3	0.734	CC1	11.6	0.250	2	28.7	5.99	22.8	CPM	N	…
J11504306+3312180	1	…	CC2	…	…	0	…	…	…	SE	N	…
J11504306+3312180	1	…	CC3	…	…	0	…	…	…	SE	N	…
J12115308+1249135	1	…	CC1	…	…	0	…	…	…	SE	N	…
J12121136+4849032	1	…	CC1	…	…	0	…	…	…	SE	Y	WDS
J12161505+5053376	1	…	CC1	…	…	0	…	…	…	SE	N	…
J12174539+0653230	1	…	CC1	…	…	0	…	…	…	SE	N	…
J12225061–0404462	1	…	CC1	…	…	0	…	…	…	SE	Y	Bo15b
J13020587+1222215	3	0.970	CC1	20.6	0.483	2	46.7	6.46	40.3	CPM	Y	WDS

Table 5
(Continued)

2MASS Name	$N_{\rm epochs}$	Δt (yr)	Cand. Comp.	χ^2_ν (BG)	χ^2_ν (CPM)	ν	BIC (BG)	BIC (CPM)	ΔBIC	Comp?[a]	Known Binary?	Binary Reference
J13034595+2837205	1	⋯	CC1	⋯	⋯	0	⋯	⋯	⋯	SE	N	⋯
J13061537+2043444	1	⋯	CC1	⋯	⋯	0	⋯	⋯	⋯	SE	Y	WDS
J13120689+3213179	1	⋯	CC1	⋯	⋯	0	⋯	⋯	⋯	SE	Y	Ja12
J13151846–0249516	1	⋯	CC1	⋯	⋯	0	⋯	⋯	⋯	SE	Y	Ja12
J13162169+2905548	2	0.241	CC1	0.378	1.29	1	3.84	4.75	−0.908	BG?	N	⋯
J13162169+2905548	2	0.241	CC2	0.0900	0.118	1	3.56	3.58	−0.0276	BG?	Y	WDS
J13252836+3743098	4	0.973	CC1	45.2	9.92	3	142	36.7	106	CPM	Y	WDS
J13260267+2735021	1	⋯	CC1	⋯	⋯	0	⋯	⋯	⋯	SE	N	⋯
J13282890+0514353	1	⋯	CC1	⋯	⋯	0	⋯	⋯	⋯	SE	N	⋯
J13324347+1114521	6	0.973	CC1	2.49	0.326	5	21.4	10.6	10.8	CPM	N	⋯
J13324460+1648397	1	⋯	CC1	⋯	⋯	0	⋯	⋯	⋯	SE	Y	WDS
J13373037–1048346	1	⋯	CC1	⋯	⋯	0	⋯	⋯	⋯	SE	N	⋯
J13375120+4808174	4	0.967	CC1	1.45	0.258	3	11.3	7.70	3.59	CPM	Y	WDS
J13420990–1600233	1	⋯	CC1	⋯	⋯	0	⋯	⋯	⋯	SE	Y	WDS
J13435058+5030053	3	0.967	CC1	2.84	0.264	2	11.2	6.02	5.14	CPM	N	⋯
J13474241+2127374	1	⋯	CC1	⋯	⋯	0	⋯	⋯	⋯	SE	Y	WDS
J13534589+5210298	1	⋯	CC1	⋯	⋯	0	⋯	⋯	⋯	SE	Y	Ja12
J14040922+2044314	4	0.959	CC1	1560	0.735	3	4690	9.14	4680	CPM	Y	WDS
J14105956+0751398	3	0.970	CC1	0.516	1.00	2	6.52	7.50	−0.972	BG?	N	⋯
J14141700–1521125	2	0.241	CC1	1.19	0.00	1	4.65	3.47	1.19	CPM?	N	⋯
J14170294+3142472	1	⋯	CC1	⋯	⋯	0	⋯	⋯	⋯	SE	Y	De99
J14170837+5000081	4	1.20	CC1	1.67	0.435	3	11.9	8.24	3.69	CPM	N	⋯
J14243178–0257158	1	⋯	CC1	⋯	⋯	0	⋯	⋯	⋯	SE	N	⋯
J14303394+0305440	1	⋯	CC1	⋯	⋯	0	⋯	⋯	⋯	SE	N	⋯
J14373999+6745316	2	⋯	CC1	0.358	0.360	1	3.82	3.83	−0.00247	BG?	N	⋯
J14433804–0414354	2	0.244	CC1	1.60	0.692	1	5.06	4.16	0.904	CPM?	Y	Ja12
J14445989+5309251	1	⋯	CC1	⋯	⋯	0	⋯	⋯	⋯	SE	N	⋯
J14514497–0530407	1	⋯	CC1	⋯	⋯	0	⋯	⋯	⋯	SE	N	⋯
J15005557+4525343	1	⋯	CC1	⋯	⋯	0	⋯	⋯	⋯	SE	Y	WDS
J15072382+4333531	4	0.973	CC1	7.35	2.28	3	29.0	13.8	15.2	CPM	N	⋯
J15114542+1014222	1	⋯	CC1	⋯	⋯	0	⋯	⋯	⋯	SE	Y	WDS
J15123818+4543464	3	1.19	CC1	165.	0.0800	2	336	5.65	331	CPM	Y	Mc01
J15154371–0725208	1	⋯	CC1	⋯	⋯	0	⋯	⋯	⋯	SE	N	⋯
J15233660+3837489	5	1.20	CC1	10.1	2.38	4	48.4	17.6	30.8	CPM	N	⋯
J15402840–1841460	1	⋯	CC1	⋯	⋯	0	⋯	⋯	⋯	SE	Y	WDS
J15422038+5936528	5	0.967	CC1	4.88	3.88	4	27.6	23.6	3.99	CPM	N	⋯
J15424184+8005306	2	0.244	CC1	0.837	0.625	1	4.30	4.09	0.212	CPM?	N	⋯
J15452354+7514548	1	⋯	CC1	⋯	⋯	0	⋯	⋯	⋯	SE	N	⋯
J15521824+3414537	3	1.20	CC1	7.31	2.03	2	20.1	9.56	10.5	CPM	N	⋯
J15553178+3512028	5	1.19	CC1	18.7	0.694	4	82.7	10.8	71.9	CPM	Y	Mc01
J15553178+3512028	1	⋯	CC2	⋯	⋯	0	⋯	⋯	⋯	SE	N	⋯
J15575497+6010263	4	0.964	CC1	2.41	0.589	3	14.2	8.70	5.48	CPM	N	⋯
J16015690+1825127	1	⋯	CC1	⋯	⋯	0	⋯	⋯	⋯	SE	N	⋯
J16043736+7022142	1	⋯	CC1	⋯	⋯	0	⋯	⋯	⋯	SE	N	⋯
J16060319+0333215	3	0.970	CC1	17.9	2.28	2	41.2	10.1	31.2	CPM	N	⋯
J16102225+4509347	4	0.970	CC1	0.633	0.850	3	8.83	9.48	−0.651	BG?	N	⋯
J16171135+7733477	1	⋯	CC1	⋯	⋯	0	⋯	⋯	⋯	SE	N	⋯

Table 5
(Continued)

2MASS Name	$N_{\rm epochs}$	Δt (yr)	Cand. Comp.	χ^2_ν (BG)	χ^2_ν (CPM)	ν	BIC (BG)	BIC (CPM)	ΔBIC	Comp?[a]	Known Binary?	Binary Reference
J16250150–1215254	1	⋯	CC1	⋯	⋯	0	⋯	⋯	⋯	SE	N	⋯
J16455062+0343014	6	0.970	CC1	0.937	0.224	5	13.6	10.1	3.57	CPM	N	⋯
J16510995+3555071	4	0.967	CC1	8.18	0.971	3	31.5	9.85	21.6	CPM	Y	Ja12
J16582055+0733079	2	0.00549	CC1	1.02	1.00	1	4.49	4.47	0.0177	CPM?	N	⋯
J17021204+5103284	3	0.877	CC1	4.10	0.753	2	13.7	7.00	6.69	CPM	Y	Ja12
J17035283+3211456	3	0.246	CC1	1.24	0.914	2	7.97	7.32	0.648	CPM?	Y	Dae07
J17152512+1328342	1	⋯	CC1	⋯	⋯	0	⋯	⋯	⋯	SE	N	⋯
J17183470+3400290	2	0.00281	CC1	8.05	8.04	1	11.5	11.5	0.00714	CPM?	N	⋯
J17340562+4447082	3	1.19	CC1	2.76	1.38	2	11.0	8.26	2.75	CPM?	N	⋯
J17380077+3329457	3	1.19	CC1	4.32	0.141	2	14.1	5.77	8.36	CPM	Y	Ja12
J17530062+1655029	1	⋯	CC1	⋯	⋯	0	⋯	⋯	⋯	SE	N	⋯
J17544786+4109310	5	0.734	CC1	0.627	0.511	4	10.6	10.1	0.465	CPM?	N	⋯
J18132028+0751536	1	⋯	CC1	⋯	⋯	0	⋯	⋯	⋯	SE	N	⋯
J18254891+0409280	1	⋯	CC1	⋯	⋯	0	⋯	⋯	⋯	SE	N	⋯
J18320290+2030581	2	0.0137	CC1	1.20	1.33	1	4.67	4.79	−0.127	BG?	Y	La08
J19011166+2550384	1	⋯	CC1	⋯	⋯	0	⋯	⋯	⋯	SE	N	⋯
J19031729+6359341	1	⋯	CC1	⋯	⋯	0	⋯	⋯	⋯	SE	N	⋯
J19133270+5644363	1	⋯	CC1	⋯	⋯	0	⋯	⋯	⋯	SE	N	⋯
J19205158+1903362	1	⋯	CC1	⋯	⋯	0	⋯	⋯	⋯	SE	N	⋯
J19370113+3147214	2	0.784	CC1	2.81	4.22	1	6.28	7.68	−1.41	BG?	N	⋯
J19433674+3225206	1	⋯	CC1	⋯	⋯	0	⋯	⋯	⋯	SE	N	⋯
J19471438+6402377	1	⋯	CC1	⋯	⋯	0	⋯	⋯	⋯	SE	N	⋯
J19515537+3811071	1	⋯	CC1	⋯	⋯	0	⋯	⋯	⋯	SE	N	⋯
J19543755+2013065	1	⋯	CC1	⋯	⋯	0	⋯	⋯	⋯	SE	N	⋯
J20013373+2814101	3	1.61	CC1	1.40	0.259	2	8.30	6.01	2.29	CPM?	Y	WDS
J20194925+2256367	1	⋯	CC1	⋯	⋯	0	⋯	⋯	⋯	SE	N	⋯
J20322012+5047455	1	⋯	CC1	⋯	⋯	0	⋯	⋯	⋯	SE	N	⋯
J20393474+4822450	2	0.896	CC1	0.738	0.160	1	4.20	3.63	0.578	CPM?	N	⋯
J20395460+0620118	1	⋯	CC1	⋯	⋯	0	⋯	⋯	⋯	SE	N	⋯
J20422203+5311332	1	⋯	CC1	⋯	⋯	0	⋯	⋯	⋯	SE	N	⋯
J20424915+4122599	2	0.101	CC1	9.17	5.16	1	12.6	8.63	4.01	CPM	N	⋯
J20560274–1710538	1	⋯	CC1	⋯	⋯	0	⋯	⋯	⋯	SE	Y	Jay01
J21000529+4004136	1	⋯	CC1	⋯	⋯	0	⋯	⋯	⋯	SE	Y	WDS
J21010182+2615397	1	⋯	CC1	⋯	⋯	0	⋯	⋯	⋯	SE	N	⋯
J21143673+1952557	4	1.04	CC1	3.14	0.0185	3	16.4	6.99	9.37	CPM	N	⋯
J21175904+3404301	2	0.896	CC1	0.969	0.100	1	4.43	3.57	0.869	CPM?	N	⋯
J21294054+6405399	1	⋯	CC1	⋯	⋯	0	⋯	⋯	⋯	SE	N	⋯
J21322198+2433419	1	⋯	CC1	⋯	⋯	0	⋯	⋯	⋯	SE	Y	Mc01
J21363852+3927206	1	⋯	CC1	⋯	⋯	0	⋯	⋯	⋯	SE	Y	WDS
J21374019+0137137	1	⋯	CC1	⋯	⋯	0	⋯	⋯	⋯	SE	Y	Ja14b
J21411161–1011001	1	⋯	CC1	⋯	⋯	0	⋯	⋯	⋯	SE	N	⋯
J21501406+0922295	1	⋯	CC1	⋯	⋯	0	⋯	⋯	⋯	SE	N	⋯
J21512893–0238147	1	⋯	CC1	⋯	⋯	0	⋯	⋯	⋯	SE	N	⋯
J21521039+0537356	1	⋯	CC1	⋯	⋯	0	⋯	⋯	⋯	SE	Y	Jo13
J21543507+5445122	1	⋯	CC1	⋯	⋯	0	⋯	⋯	⋯	SE	Y	WDS
J21552437+5938371	1	⋯	CC1	⋯	⋯	0	⋯	⋯	⋯	SE	Y	Ja14b
J22073842–0650034	1	⋯	CC1	⋯	⋯	0	⋯	⋯	⋯	SE	N	⋯

Table 5
(Continued)

2MASS Name	$N_{\rm epochs}$	Δt (yr)	Cand. Comp.	χ^2_ν (BG)	χ^2_ν (CPM)	ν	BIC (BG)	BIC (CPM)	ΔBIC	Comp?[a]	Known Binary?	Binary Reference
J22300418+4851347	1	…	CC1	…	…	0	…	…	…	SE	Y	Ja14b
J22413501+1849277	1	…	CC1	…	…	0	…	…	…	SE	N	…
J22413577+2602128	3	1.08	CC1	2.32	3.10	2	10.1	11.7	−1.57	BG?	N	…
J22424884+1330532	1	…	CC1	…	…	0	…	…	…	SE	Y	WDS
J22594127+2154070	4	0.320	CC1	0.224	0.183	3	7.60	7.48	0.123	CPM?	N	…
J23002791–2618431	1	…	CC1	…	…	0	…	…	…	SE	Y	WDS
J23024391+7506019	1	…	CC1	…	…	0	…	…	…	SE	Y	WDS
J23040837+0318214	3	0.0986	CC1	0.156	0.355	2	5.80	6.20	−0.398	BG?	N	…
J23040837+0318214	1	…	CC2	…	…	0	…	…	…	SE	N	…
J23060295–1556151	1	…	CC1	…	…	0	…	…	…	SE	N	…
J23062378+1236269	2	0.726	CC1	34.4	1.61	1	37.9	5.08	32.8	CPM	Y	WDS
J23220944+5756296	1	…	CC1	…	…	0	…	…	…	SE	N	…
J23450477+1458573	2	0.326	CC1	2.72	0.256	1	6.19	3.72	2.47	CPM?	Y	Ja12
J23473777–2316060	1	…	CC1	…	…	0	…	…	…	SE	N	…
J23574989+3837468	2	1.03	CC1	14.6	0.920	1	18.1	4.39	13.7	CPM	Y	Mc01
J23581366–1724338	1	…	CC1	…	…	0	…	…	…	SE	Y	Dae07
J23590042+2051387	1	…	CC1	…	…	0	…	…	…	SE	N	…

Note.
[a] Status of companion based on differenced Bayesian Information Criterion for the common proper motion and background hypotheses. "SE"—Single Epoch; "BG"—background; "CPM"—Common Proper Motion. See Section 4.2 for details.

References. Beu04—Beuzit et al. (2004), Ber10—Bergfors et al. (2010), Bo15a—Bowler et al. (2015b), Bo15b—Bowler et al. (2015a), Dae07—Daemgen et al. (2007), De99—Delfosse et al. (1999), Gu05—Guenther et al. (2005), Ja12—Janson et al. (2012), Ja14b—Janson et al. (2014a), Jay01—Jayawardhana & Brandeker (2001), Jo13—Jodar et al. (2013), La08—Law et al. (2008), Mc01—McCarthy et al. (2001), Sc98—Schneider et al. (1998), WDS—Mason et al. (2001).

(This table is available in its entirety in machine-readable form.)

Table 6
Properties of Robo-AO Visual Binaries

2MASS Name	$\mu_\alpha \cos(\delta)$[a] (mas yr^{-1})	μ_δ[a] (mas yr^{-1})	Distance[a] (pc)	Cand. Comp.	Proj. Sep. ($''$)	BANYAN Σ Best Hyp.	Literature YMG	YMG Reference
J00074264+6022543	321.81 ± 1.48	−5.61 ± 1.18	16.48 ± 0.25	CC1	0.86	Field	⋯	⋯
J00133841+5245050	61.36 ± 0.04	−42.18 ± 0.03	54.63 ± 0.09	CC1/CC2	3.13/0.86	Field	⋯	⋯
J00160486+2319090	140.26 ± 0.14	−45.65 ± 0.17	37.88 ± 0.14	CC1	2.66	Field	⋯	⋯
J00164045+3000598	223.82 ± 0.29	23.70 ± 0.21	41.56 ± 0.30	CC1	0.98	Field	⋯	⋯
J00165678+2003551	212.24 ± 0.44	−28.39 ± 0.58	39.06 ± 0.38	CC1	1.03	Field	⋯	⋯
J00171046+2931520	76.01 ± 0.08	−90.22 ± 0.06	54.96 ± 0.16	CC1	1.02	AB Dor	⋯	⋯
J00215781+4912379	208.77 ± 0.10	−35.03 ± 0.07	29.56 ± 0.05	CC1/CC2	2.29/2.66	Field	Car?	Shk12
J00233468+2014282	65.97 ± 0.10	−37.38 ± 0.11	62.89 ± 0.25	CC1	1.73	Field	β Pic	Le09, Ma13, Ma14a, Sh17
J00285391+5022330	447.86 ± 1.18	132.93 ± 0.94	13.48 ± 0.17	CC1	0.32	Field	⋯	⋯
J00302927+0420204	72.51 ± 0.08	−1.00 ± 0.05	59.35 ± 0.15	CC1	1.70	Field	⋯	⋯
J00323480+0729271	104.47 ± 0.29	−63.63 ± 0.18	35.60 ± 0.20	CC1	0.71	β Pic	β Pic?	Sch12b, Sch12a, Bi15a, Me17
J00340843+2523498	82.28 ± 0.18	−97.32 ± 0.08	47.68 ± 0.28	CC1	1.54	AB Dor	AB Dor	Sch10, Ma13, Ma14a
J00414141+4410530	−44.5 ± 2.4[b]	−27.1 ± 2.9[b]	⋯	CC1	0.51	Field	⋯	⋯
J00423409+5439048	140.72 ± 0.19	−12.91 ± 0.24	57.44 ± 0.59	CC1	2.98	Field	⋯	⋯
J00425668+2239350	400.51 ± 0.37	21.95 ± 0.25	31.68 ± 0.12	CC1	2.96	Field	⋯	⋯
J00485822+4435091	120.30 ± 1.82	−130.67 ± 1.24	32.99 ± 0.87	CC1	0.97	AB Dor	AB Dor	Sch12a, Sch12b
J00503319+2449009	203.42 ± 0.23	−31.92 ± 0.18	14.97 ± 0.03	CC1	0.94	Field	Arg	Ma14a
J00530648+4829385	229.28 ± 0.14	−143.59 ± 0.17	65.24 ± 0.46	CC1	1.31	Field	⋯	⋯
J01001331+2135328	77.77 ± 0.14	12.67 ± 0.25	82.07 ± 0.68	CC1	2.63	Field	⋯	⋯
J01001613+1251007	47.41 ± 0.08	−31.57 ± 0.06	94.15 ± 0.41	CC1	1.10	Field	⋯	⋯
J01034013+4051288	116.61 ± 0.12	−161.31 ± 0.12	31.06 ± 0.08	CC1	2.53	AB Dor	AB Dor	Shk12
J01071194–1935359	64.4 ± 1.6[b]	−39.5 ± 1.2[b]	⋯	CC1	0.47	Field	β Pic/Tuc-Hor/Col?	Ki10, Pe13, Ma13, Kr14, Sh17
J01093915+2931112	150.8 ± 4.8[b]	5.8 ± 5.3[b]	⋯	CC1	0.56	Field	⋯	⋯
J01102943–1510071	174.19 ± 0.10	23.95 ± 0.08	43.51 ± 0.10	CC1	2.38	Field	⋯	⋯
J01105436+5822133	85.25 ± 0.23	−50.22 ± 0.25	44.54 ± 0.45	CC1	0.73	Field	⋯	⋯
J01112542+1526214	192.0 ± 8.0[b]	−130.0 ± 8.0[b]	⋯	CC1	0.33	Col	β Pic	Ma13, Ma14b, Ri14, Sh17
J01121854+4238358	93.74 ± 0.09	17.82 ± 0.08	100.11 ± 0.57	CC1/CC2	2.94/0.73	Field	⋯	⋯
J01131976+5855224	163.84 ± 0.04	−132.77 ± 0.05	27.71 ± 0.03	CC1	2.08	AB Dor	AB Dor?	Sch12a
J01132958–0738088	74.65 ± 0.08	−68.29 ± 0.06	65.08 ± 0.22	CC1	3.02	Field	AB Dor?	Ma13
J01244246–1540454	188.2 ± 8.0[b]	−22.8 ± 8.0[b]	⋯	CC1	0.26	Field	⋯	⋯
J01281337–2319278	207.97 ± 0.16	−5.95 ± 0.14	60.94 ± 0.29	CC1	1.11	Field	⋯	⋯
J01304065–1027506	120.56 ± 2.03	4.37 ± 1.33	33.95 ± 1.57	CC1	0.96	Field	⋯	⋯
J01373940+1835332	74.76 ± 0.22	−43.35 ± 0.15	52.15 ± 0.28	CC1	1.71	β Pic	β Pic/Col?	Sch10, Ma14b, Sh17
J01535076–1459503	106.65 ± 0.17	−40.79 ± 0.21	33.84 ± 0.14	CC1	2.87	β Pic	β Pic	Ma13, Ma14a, Sh17
J01592349+5831162	320.58 ± 0.10	−192.69 ± 0.10	13.13 ± 0.01	CC1/CC2	3.96/1.71	Col	Car/Col?	Shk12, Br14
J02155892–0929121	96.6 ± 1.9[b]	−46.5 ± 2.6[b]	⋯	CC1/CC2	0.51/3.36	Tuc-Hor	Tuc-Hor/β Pic?/Col?	Ma13, Kr14, Bo15a, Na17
J02205082+3320479	144.35 ± 0.09	−111.33 ± 0.09	53.11 ± 0.14	CC1	1.50	Field	⋯	⋯
J02233670–1056138	99.61 ± 0.07	−41.99 ± 0.08	121.33 ± 0.61	CC1	2.66	Field	⋯	⋯
J02284694+1538535	170.91 ± 0.18	−9.17 ± 0.17	35.05 ± 0.14	CC1	0.84	Field	⋯	⋯

Table 6
(Continued)

2MASS Name	$\mu_\alpha \cos(\delta)$[a] (mas yr^{-1})	μ_δ[a] (mas yr^{-1})	Distance[a] (pc)	Cand. Comp.	Proj. Sep. ($''$)	BANYAN Σ Best Hyp.	Literature YMG	YMG Reference
J02335984–1811525	72.97 ± 0.79	−30.34 ± 0.62	80.56 ± 2.67	CC1	0.87	Field	Col/β Pic	Ro13, Ma14a, Sh17
J02490228–1029220	44.1 ± 1.9[b]	−21.7 ± 2.3[b]	⋯	CC1	0.72	Field	β Pic?	Ber15
J02560096+1220457	162.0 ± 8.0[b]	−67.0 ± 8.0[b]	⋯	CC1	0.89	Field	⋯	⋯
J03033668–2535329	217.89 ± 0.30	106.94 ± 0.31	35.44 ± 0.20	CC1	0.85	Field	Arg	Ma13
J03092643+6732425	−67.07 ± 0.35	54.41 ± 0.44	50.54 ± 0.71	CC1	2.78	Field	⋯	⋯
J03144720+1127272	60.98 ± 0.67	−46.18 ± 0.48	58.90 ± 0.96	CC1	0.59	Field	⋯	⋯
J03175221+5847431	72.68 ± 0.04	−6.71 ± 0.06	100.28 ± 0.34	CC1	2.43	Field	⋯	⋯
J03240643+2347073	215.05 ± 0.10	−120.24 ± 0.07	20.71 ± 0.02	CC1	2.63	Car-Near	Car-Near?, Arg	Zu06, El16
J03323578+2843554	58.8 ± 2.6[b]	−81.0 ± 3.5[b]	⋯	CC1	0.47	β Pic	β Pic?	Sch12a, Ma14a, Ja14, Sh17
J03340048+5835551	292.12 ± 0.68	−172.80 ± 0.51	39.16 ± 0.65	CC1	0.81	Field	⋯	⋯
J03434696+5725557	−84.37 ± 0.06	42.56 ± 0.06	29.45 ± 0.03	CC1	3.54	Field	⋯	⋯
J03520223+2439479	31.15 ± 0.93	−41.46 ± 0.87	450.29 ± 161.04	CC1	0.45	Field	Pleiades	St07
J04053888+0544408	47.90 ± 2.03	−53.21 ± 2.04	36.73 ± 1.62	CC1	0.78	β Pic	⋯	⋯
J04074484+0945220	64.68 ± 0.88	−13.94 ± 0.58	44.66 ± 0.71	CC1	0.77	Field	⋯	⋯
J04112810+7544231	14.8 ± 2.4[b]	−29.9 ± 2.1[b]	⋯	CC1	0.27	Field	⋯	⋯
J04132663–0139211	138.76 ± 0.57	−19.20 ± 0.38	30.01 ± 0.33	CC1	0.72	Field	Arg?	Ma13
J04134585–0509049	177.39 ± 0.29	−110.10 ± 0.17	29.62 ± 0.19	CC1	3.37	Field	⋯	⋯
J04171645+1213557	31.4 ± 1.9[b]	−11.8 ± 1.9[b]	⋯	CC1	0.73	Field	⋯	⋯
J04174337–1754222	27.77 ± 0.04	17.10 ± 0.04	73.31 ± 0.19	CC1	2.78	Field	⋯	⋯
J04174431+4103137	67.51 ± 0.16	−209.25 ± 0.09	30.55 ± 0.07	CC1	2.52	AB Dor	AB Dor?	Sch12a
J04214271–1657543	30.9 ± 1.7[b]	−8.0 ± 2.1[b]	⋯	CC1	0.41	Field	⋯	⋯
J04244805+1552292	121.40 ± 2.00	−17.82 ± 1.27	143.58 ± 15.23	CC1	0.31	Field	⋯	⋯
J04251456+1858250	97.98 ± 0.11	−28.35 ± 0.09	52.95 ± 0.20	CC1	0.83	Hyades	Hyades	Ro11
J04282878+1741453	108.16 ± 0.62	−41.79 ± 0.36	46.88 ± 0.57	CC1	1.71	Field	Hyades	Ro11
J04285080+1617204	101.21 ± 2.14	−10.38 ± 2.13	54.45 ± 3.41	CC1/CC2	1.97/0.73	Field	Hyades	Ro11
J04311384+2053436	23.11 ± 0.29	−114.21 ± 0.19	33.98 ± 0.16	CC1	0.65	Field	⋯	⋯
J04325718+7407002	78.38 ± 0.06	−124.92 ± 0.09	33.85 ± 0.05	CC1	2.86	Col	Col?	Ga18c
J04343992+1512325	103.56 ± 0.27	−35.76 ± 0.14	48.07 ± 0.31	CC1	1.05	Field	Hyades	Ro11
J04350255+0839304	90.95 ± 1.26	−0.74 ± 0.96	59.34 ± 2.64	CC1	0.32	Hyades	Hyades	Ro11
J04381255+2813001	395.65 ± 0.97	−92.04 ± 0.79	13.62 ± 0.09	CC1	1.15	Field	⋯	⋯
J04385352+2147549	187.71 ± 0.64	−213.61 ± 0.47	41.00 ± 0.65	CC1	1.27	Field	⋯	⋯
J04412780+1404340	95.71 ± 0.92	−23.97 ± 0.65	49.21 ± 1.24	CC1	0.26	Hyades	Hyades	Ro11
J04485498+5527185	91.74 ± 0.93	−105.93 ± 0.88	43.59 ± 1.27	CC1	0.51	Field	⋯	⋯
J04492947+4828459	180.0 ± 8.0[b]	−195.0 ± 8.0[b]	⋯	CC1	0.63	Field	⋯	⋯
J04495635+2341029	37.18 ± 0.19	−170.12 ± 0.11	41.05 ± 0.16	CC1	2.46	AB Dor	⋯	⋯
J05024924+7352143	47.67 ± 1.90	−56.70 ± 1.90	57.39 ± 4.50	CC1	0.34	Field	⋯	⋯
J05122408+1824086	64.29 ± 0.13	−31.91 ± 0.09	53.09 ± 0.19	CC1	1.50	Hyades	Hyades	Ro11
J05195513–0723399	62.97 ± 1.06	−47.16 ± 0.85	57.73 ± 2.10	CC1	0.53	Field	⋯	⋯
J05252028+6510544	−108.75 ± 0.04	19.51 ± 0.04	38.05 ± 0.04	CC1	1.63	Field	⋯	⋯
J05285650+1231539	93.0 ± 8.0[b]	−211.0 ± 8.0[b]	⋯	CC1	0.23	Col	⋯	⋯
J05341064+4732033	−58.07 ± 0.07	36.85 ± 0.06	33.25 ± 0.05	CC1	2.47	Field	⋯	⋯
J05345873+6521435	47.63 ± 0.09	−118.80 ± 0.11	52.15 ± 0.21	CC1	1.17	Field	⋯	⋯
J05494518+2513331	12.68 ± 0.10	−47.88 ± 0.08	103.46 ± 0.62	CC1	2.89	Field	⋯	⋯
J05554690+5123592	34.31 ± 0.06	−105.94 ± 0.05	60.88 ± 0.14	CC1	1.88	Field	⋯	⋯
J06073185+4712266	37.77 ± 0.16	−188.43 ± 0.14	28.30 ± 0.09	CC1	3.45	Col	AB Dor?	Sch12a
J06084814+4257182	39.22 ± 0.12	−238.52 ± 0.10	47.62 ± 0.14	CC1	1.29	Field	⋯	⋯
J06101580+2119569	54.64 ± 0.24	−193.47 ± 0.20	59.12 ± 0.30	CC1/CC2	1.93/1.28	Field	⋯	⋯
J06133437+4914051	33.20 ± 0.44	−39.40 ± 0.42	90.54 ± 2.29	CC1	0.79	Field	⋯	⋯
J06462622+0521150	59.68 ± 0.08	−0.69 ± 0.07	42.84 ± 0.09	CC1	4.17	Field	⋯	⋯
J06584690+2843004	−30.11 ± 1.24	−116.93 ± 1.10	41.75 ± 1.21	CC1	1.03	Field	⋯	⋯
J07120481+5423473	12.61 ± 0.81	−108.40 ± 0.66	76.90 ± 3.81	CC1	1.04	Field	⋯	⋯
J07140450+5043334	−130.35 ± 0.05	−269.34 ± 0.04	28.43 ± 0.03	CC1/CC2	1.90/1.11	Field	⋯	⋯
J07161207+3315154	−80.56 ± 0.10	−182.04 ± 0.07	28.62 ± 0.06	CC1	1.84	Field	⋯	⋯
J07194218+2954390	−22.79 ± 0.81	−90.88 ± 0.73	52.16 ± 1.32	CC1	0.48	Field	⋯	⋯
J07315773+3613102	−249.50 ± 0.08	−246.33 ± 0.07	12.00 ± 0.01	CC1	1.58	Field	⋯	⋯

Table 6
(Continued)

2MASS Name	$\mu_\alpha \cos(\delta)$[a] (mas yr^{-1})	μ_δ[a] (mas yr^{-1})	Distance[a] (pc)	Cand. Comp.	Proj. Sep. ($''$)	BANYAN Σ Best Hyp.	Literature YMG	YMG Reference
J07505369+4428181	66.25 ± 0.06	−140.52 ± 0.05	49.98 ± 0.09	CC1	2.11	Field	⋯	⋯
J08010582+0334064	−176.78 ± 0.08	−124.53 ± 0.05	46.96 ± 0.10	CC1	2.25	Field	⋯	⋯
J08014318+4959455	−77.62 ± 0.36	−68.60 ± 0.25	56.63 ± 0.85	CC1	1.16	Field	⋯	⋯
J08083284+5304377	−89.35 ± 0.32	−91.10 ± 0.30	35.00 ± 0.31	CC1	1.23	Field	⋯	⋯
J08095207+0301106	−15.16 ± 0.06	−39.24 ± 0.04	97.73 ± 0.34	CC1	2.43	Field	⋯	⋯
J08310177+4012115	−88.34 ± 0.09	−124.43 ± 0.07	33.67 ± 0.07	CC1	1.94	Field	⋯	⋯
J08444213+0044159	−108.18 ± 0.07	−9.32 ± 0.04	65.04 ± 0.16	CC1	3.26	Field	⋯	⋯
J08504234+0751517	−43.41 ± 0.10	−26.49 ± 0.07	17.80 ± 0.02	CC1	1.21	Field	⋯	⋯
J08593592+5343505	−268.16 ± 1.92	−194.23 ± 1.69	13.46 ± 0.19	CC1	0.37	Field	⋯	⋯
J09062111+1659235	−96.6 ± 1.6[b]	−34.2 ± 2.0[b]	⋯	CC1	0.88	Field	⋯	⋯
J09132383+6852305	−154.9 ± 2.3[b]	−233.2 ± 2.2[b]	⋯	CC1	0.60	AB Dor	AB Dor?	Sch12a, Ga18b
J09174473+4612246	−129.87 ± 0.70	−17.50 ± 0.75	33.45 ± 0.48	CC1	0.19	Field	⋯	⋯
J09192291+6203170	−288.35 ± 0.06	−386.15 ± 0.08	38.10 ± 0.07	CC1	0.79	Field	⋯	⋯
J09200048+3052397	−74.3 ± 6.0[b]	−33.6 ± 3.3[b]	⋯	CC1	0.42	Field	⋯	⋯
J09214911+4330284	−295.0 ± 8.0[b]	−121.0 ± 8.0[b]	⋯	CC1	0.71	Field	⋯	⋯
J10024936+4827333	−321.0 ± 8.0[b]	−280.0 ± 8.0[b]	⋯	CC1	0.20	Field	⋯	⋯
J10043276+0533412	−77.7 ± 1.7[b]	−102.2 ± 2.2[b]	⋯	CC1	0.30	AB Dor	⋯	⋯
J10143153+0213174	−29.73 ± 0.39	−46.01 ± 0.46	85.23 ± 1.27	CC1	0.67	Field	⋯	⋯
J10143194+0606409	−144.00 ± 0.09	−69.54 ± 0.09	32.36 ± 0.06	CC1	2.13	Field	⋯	⋯
J10150690+3125110	−55.05 ± 0.11	−213.17 ± 0.15	33.56 ± 0.08	CC1	1.81	Field	⋯	⋯
J10452148+3830422	−38.26 ± 0.29	154.35 ± 0.45	13.70 ± 0.05	CC1	0.68	Field	⋯	⋯
J10482887+5852005	−199.46 ± 0.04	−55.92 ± 0.05	43.91 ± 0.06	CC1/CC2	1.20/1.80	Field	⋯	⋯
J10571139+0544547	−59.14 ± 0.84	−37.78 ± 0.90	104.94 ± 4.92	CC1	1.01	Field	β Pic?	Sch12c
J11030845+1517518	−419.0 ± 8.0[b]	−84.0 ± 8.0[b]	⋯	CC1	0.39	Car-Near	⋯	⋯
J11161238+4942112	−74.48 ± 0.46	−0.37 ± 0.49	79.19 ± 2.29	CC1	0.79	Field	⋯	⋯
J11432359+2518137	−233.0 ± 8.0[b]	−31.0 ± 8.0[b]	⋯	CC1	0.48	Car-Near	⋯	⋯
J11470543+7001588	−342.70 ± 0.69	−33.53 ± 0.64	30.68 ± 0.37	CC1	0.91	Field	⋯	⋯
J11474897+0459160	−134.93 ± 0.09	−95.43 ± 0.06	38.03 ± 0.08	CC1	1.68	Field	⋯	⋯
J11503435+2903407	−213.0 ± 10.2[b]	18.4 ± 6.3[b]	⋯	CC1	0.51	Field	⋯	⋯
J11504306+3312180	−209.71 ± 1.44	5.62 ± 1.62	49.01 ± 1.97	CC1/CC2/CC3	0.59/2.58/0.49	Field	⋯	⋯
J12115308+1249135	−71.62 ± 0.13	−57.64 ± 0.07	61.02 ± 0.30	CC1	1.17	Field	β Pic?	Sch12a
J12121136+4849032	197.82 ± 0.03	−314.46 ± 0.04	26.59 ± 0.02	CC1	2.85	Field	⋯	⋯
J12161505+5053376	−79.57 ± 0.07	34.16 ± 0.09	38.04 ± 0.10	CC1	1.90	Field	⋯	⋯
J12174539+0653230	−103.31 ± 0.10	42.01 ± 0.05	49.48 ± 0.11	CC1	2.63	Field	⋯	⋯
J12225061–0404462	−255.0 ± 8.0[b]	−65.7 ± 8.0[b]	⋯	CC1	0.24	Field	⋯	⋯
J13020587+1222215	−217.30 ± 0.20	−95.69 ± 0.12	30.22 ± 0.07	CC1	2.93	Field	⋯	⋯
J13034595+2837205	−33.15 ± 0.05	20.25 ± 0.04	214.34 ± 1.67	CC1	1.86	Field	⋯	⋯
J13061537+2043444	−55.82 ± 0.07	94.57 ± 0.05	19.65 ± 0.02	CC1	1.61	Field	⋯	⋯
J13120689+3213179	114.5 ± 2.3[b]	−89.0 ± 4.0[b]	⋯	CC1	0.24	Field	⋯	⋯
J13151846–0249516	165.2 ± 8.0[b]	−165.2 ± 8.0[b]	⋯	CC1	0.29	Field	⋯	⋯
J13162169+2905548	−157.77 ± 0.09	−107.31 ± 0.10	59.68 ± 0.26	CC1/CC2	0.29/2.42	Field	⋯	⋯
J13252836+3743098	−197.94 ± 0.05	57.35 ± 0.04	33.79 ± 0.04	CC1	2.91	Field	⋯	⋯
J13260267+2735021	−2.97 ± 0.17	73.12 ± 0.14	45.20 ± 0.16	CC1	1.49	Field	⋯	⋯
J13282890+0514353	−63.87 ± 0.11	−51.28 ± 0.08	111.34 ± 0.68	CC1	0.93	Field	⋯	⋯
J13324347+1114521	−165.62 ± 0.11	9.66 ± 0.06	51.07 ± 0.11	CC1	1.45	Field	⋯	⋯
J13324460+1648397	287.56 ± 0.27	−206.79 ± 0.12	16.58 ± 0.03	CC1	2.83	Field	⋯	⋯
J13373037–1048346	90.5 ± 2.8[b]	−152.7 ± 2.4[b]	⋯	CC1	0.41	Field	⋯	⋯
J13375120+4808174	−241.53 ± 0.05	−137.72 ± 0.05	21.19 ± 0.01	CC1	1.63	Field	⋯	⋯
J13420990–1600233	−496.64 ± 0.70	−49.15 ± 0.58	21.06 ± 0.23	CC1	0.62	Field	⋯	⋯
J13435058+5030053	−80.04 ± 0.49	−10.50 ± 0.53	62.45 ± 1.49	CC1	1.08	Field	⋯	⋯
J13474241+2127374	79.92 ± 0.08	−89.26 ± 0.06	29.94 ± 0.04	CC1	1.33	Field	⋯	⋯
J13534589+5210298	−2.78 ± 1.40	−130.26 ± 1.42	56.15 ± 2.83	CC1	1.06	Field	⋯	⋯
J14040922+2044314	−130.5 ± 3.3[b]	−20.4 ± 1.8[b]	⋯	CC1	0.43	Field	⋯	⋯
J14105956+0751398	−51.03 ± 0.14	9.05 ± 0.13	34.27 ± 0.11	CC1	1.38	Field	⋯	⋯
J14141700–1521125	−120.12 ± 0.11	−197.14 ± 0.10	28.65 ± 0.05	CC1	1.61	AB Dor	β Pic?	El16, Sh17
J14170294+3142472	−589.0 ± 8.0[b]	−143.0 ± 8.0[b]	⋯	CC1	0.27	Field	⋯	⋯
J14170837+5000081	−105.79 ± 0.13	42.29 ± 0.12	64.36 ± 0.36	CC1	1.70	Field	⋯	⋯
J14243178–0257158	−66.95 ± 0.55	−33.15 ± 0.46	131.53 ± 4.92	CC1	3.85	Field	⋯	⋯

Table 6
(Continued)

2MASS Name	$\mu_\alpha \cos(\delta)$[a] (mas yr^{-1})	μ_δ[a] (mas yr^{-1})	Distance[a] (pc)	Cand. Comp.	Proj. Sep. ($''$)	BANYAN Σ Best Hyp.	Literature YMG	YMG Reference
J14303394+0305440	44.15 ± 0.85	11.18 ± 0.78	57.41 ± 1.36	CC1	2.69	Field	⋯	⋯
J14373999+6745316	−213.52 ± 0.67	184.48 ± 0.73	41.03 ± 0.53	CC1	0.88	Field	⋯	⋯
J14433804–0414354	−101.85 ± 0.29	−69.61 ± 0.28	51.62 ± 0.53	CC1	1.01	Field	⋯	⋯
J14445989+5309251	−102.14 ± 1.00	11.01 ± 1.10	58.93 ± 2.17	CC1	0.86	Field	⋯	⋯
J14514497–0530407	−63.37 ± 0.74	−2.92 ± 0.86	83.81 ± 2.88	CC1	0.48	Field	⋯	⋯
J15005557+4525343	224.77 ± 0.06	328.98 ± 0.06	11.71 ± 0.01	CC1	2.03	Field	⋯	⋯
J15072382+4333531	79.64 ± 0.88	39.88 ± 1.07	30.83 ± 0.55	CC1	0.55	Field	⋯	⋯
J15114542+1014222	−35.99 ± 0.12	22.12 ± 0.08	108.90 ± 0.56	CC1	1.92	Field	⋯	⋯
J15123818+4543464	−387.0 ± 8.0[b]	352.0 ± 8.0[b]	⋯	CC1	0.54	Field	⋯	⋯
J15154371–0725208	−150.7 ± 4.3[b]	−277.8 ± 9.3[b]	⋯	CC1	0.60	AB Dor	⋯	⋯
J15233660+3837489	−108.0 ± 1.2[b]	−51.2 ± 1.5[b]	⋯	CC1	0.62	AB Dor	AB Dor?	Sch12a
J15402840–1841460	−60.85 ± 0.58	−148.75 ± 0.36	38.15 ± 0.38	CC1	0.76	AB Dor	AB Dor	Zu04, To08
J15422038+5936528	−88.40 ± 0.06	20.80 ± 0.08	44.52 ± 0.07	CC1	1.58	Field	⋯	⋯
J15424184+8005306	−45.97 ± 0.03	67.33 ± 0.03	76.43 ± 0.11	CC1	2.08	Field	⋯	⋯
J15452354+7514548	−28.94 ± 1.69	−63.38 ± 1.80	49.50 ± 2.31	CC1	0.96	Field	⋯	⋯
J15521824+3414537	−78.99 ± 0.03	191.13 ± 0.04	45.64 ± 0.04	CC1	1.80	Field	⋯	⋯
J15553178+3512028	−232.36 ± 0.06	155.98 ± 0.09	27.82 ± 0.03	CC1/ CC2	1.61/1.87	Field	Arg?	Ma13, Ma14a
J15575497+6010263	−63.9 ± 1.4[b]	31.0 ± 0.9[b]	⋯	CC1	0.70	Field	⋯	⋯
J16015690+1825127	−36.35 ± 0.05	−87.74 ± 0.05	65.28 ± 0.22	CC1	1.25	Field	⋯	⋯
J16043736+7022142	46.60 ± 2.01	15.84 ± 2.41	48.38 ± 2.75	CC1	0.76	Field	⋯	⋯
J16060319+0333215	−104.9 ± 2.7[b]	−95.4 ± 2.6[b]	⋯	CC1	0.56	Field	⋯	⋯
J16102225+4509347	−11.05 ± 0.08	29.87 ± 0.10	100.96 ± 0.48	CC1	2.43	Field	⋯	⋯
J16171135+7733477	−38.27 ± 0.14	39.80 ± 0.18	72.57 ± 0.44	CC1	0.81	Field	AB Dor?/ β Pic?	Sch12a
J16250150–1215254	−184.8 ± 8.0[b]	−173.6 ± 8.0[b]	⋯	CC1	0.31	Field	⋯	⋯
J16455062+0343014	−37.67 ± 0.08	−105.38 ± 0.07	44.89 ± 0.08	CC1	2.06	AB Dor	AB Dor?	Sch12a, Sch12b, Bi15b
J16510995+3555071	−74.28 ± 0.12	175.23 ± 0.15	34.93 ± 0.08	CC1	1.07	Field	⋯	⋯
J16582055+0733079	35.1 ± 2.7[b]	−14.4 ± 3.4[b]	⋯	CC1	0.50	Field	⋯	⋯
J17021204+5103284	−37.50 ± 1.61	77.33 ± 1.55	60.65 ± 2.80	CC1	0.78	Field	⋯	⋯
J17035283+3211456	192.41 ± 0.64	99.97 ± 0.66	19.13 ± 0.12	CC1	1.44	Field	⋯	⋯
J17152512+1328342	30.40 ± 0.96	23.22 ± 0.92	53.97 ± 1.44	CC1	0.74	Field	⋯	⋯
J17183470+3400290	−14.62 ± 0.04	172.98 ± 0.05	50.56 ± 0.07	CC1	1.32	Field	⋯	⋯
J17340562+4447082	−97.2 ± 4.1[b]	20.1 ± 2.0[b]	⋯	CC1	0.59	Field	⋯	⋯
J17380077+3329457	−121.22 ± 0.21	54.06 ± 0.22	52.62 ± 0.32	CC1	0.97	Field	⋯	⋯
J17530062+1655029	−243.94 ± 2.13	−240.05 ± 2.24	22.65 ± 0.52	CC1	0.88	Field	⋯	⋯
J17544786+4109310	−15.03 ± 0.71	93.65 ± 0.68	67.10 ± 1.70	CC1	0.83	Field	⋯	⋯
J18132028+0751536	24.04 ± 1.47	62.82 ± 1.54	53.10 ± 3.06	CC1	0.98	Field	⋯	⋯
J18254891+0409280	7.88 ± 0.06	−90.95 ± 0.06	54.99 ± 0.10	CC1	3.62	Field	⋯	⋯
J18320290+2030581	−47.48 ± 0.27	−214.65 ± 0.40	31.20 ± 0.17	CC1	1.38	Field	⋯	⋯
J19011166+2550384	−11.18 ± 0.08	36.69 ± 0.09	48.87 ± 0.14	CC1	1.34	Field	⋯	⋯
J19031729+6359341	63.7 ± 2.5[b]	112.1 ± 1.3[b]	⋯	CC1	3.69	AB Dor	⋯	⋯
J19133270+5644363	−5.84 ± 0.33	33.94 ± 0.29	69.23 ± 0.67	CC1	1.17	Field	⋯	⋯
J19205158+1903362	67.8 ± 2.3[b]	63.9 ± 3.4[b]	⋯	CC1	0.51	Field	⋯	⋯
J19370113+3147214	80.5 ± 1.3[b]	100.5 ± 0.7[b]	⋯	CC1	0.51	Field	⋯	⋯
J19433674+3225206	43.90 ± 0.05	−5.46 ± 0.05	47.75 ± 0.07	CC1	0.40	Field	⋯	⋯
J19471438+6402377	92.18 ± 0.09	23.13 ± 0.07	67.20 ± 0.15	CC1	0.17	Field	⋯	⋯
J19515537+3811071	−14.19 ± 0.04	−143.40 ± 0.04	43.86 ± 0.05	CC1	2.32	Field	⋯	⋯
J19543755+2013065	−38.09 ± 0.04	−62.76 ± 0.04	27.42 ± 0.03	CC1	4.20	Field	⋯	⋯
J20013373+2814101	114.16 ± 0.07	79.54 ± 0.07	33.90 ± 0.06	CC1	1.54	Field	⋯	⋯
J20194925+2256367	83.53 ± 0.10	106.69 ± 0.09	29.34 ± 0.06	CC1	1.96	Field	⋯	⋯
J20322012+5047455	−10.02 ± 0.61	61.38 ± 0.63	57.40 ± 1.27	CC1	0.82	Field	⋯	⋯
J20393474+4822450	88.11 ± 0.06	48.72 ± 0.05	76.65 ± 0.20	CC1	1.86	Field	⋯	⋯
J20395460+0620118	89.41 ± 0.19	−104.27 ± 0.13	36.36 ± 0.16	CC1	2.48	Field	AB Dor	Sch10, Ma14a
J20422203+5311332	50.6 ± 1.8[b]	83.7 ± 1.8[b]	⋯	CC1	0.29	Field	⋯	⋯
J20424915+4122599	67.3 ± 1.6[b]	−31.1 ± 2.3[b]	⋯	CC1	0.48	AB Dor	AB Dor?	Sch12a
J20560274–1710538	57.31 ± 0.11	−62.14 ± 0.07	45.93 ± 0.21	CC1	2.21	β Pic	β Pic	Zu01b, To08, Sh17
J21000529+4004136	614.4 ± 8.0[b]	−247.2 ± 8.0[b]	⋯	CC1	0.89	AB Dor	⋯	⋯

Table 6
(Continued)

2MASS Name	$\mu_{\alpha}\cos(\delta)$[a] (mas yr^{-1})	μ_{δ}[a] (mas yr^{-1})	Distance[a] (pc)	Cand. Comp.	Proj. Sep. ($''$)	BANYAN Σ Best Hyp.	Literature YMG	YMG Reference
J21010182+2615397	63.5 ± 2.4[b]	−6.7 ± 2.5[b]	…	CC1	0.43	Field	…	…
J21143673+1952557	85.76 ± 0.08	−48.51 ± 0.09	122.07 ± 0.95	CC1	2.86	Field	…	…
J21175904+3404301	51.54 ± 0.08	−23.68 ± 0.10	43.48 ± 0.12	CC1	1.12	Field	…	…
J21294054+6405399	90.90 ± 0.06	28.79 ± 0.06	43.83 ± 0.07	CC1	2.44	Field	…	…
J21322198+2433419	229.54 ± 0.09	−8.71 ± 0.10	20.55 ± 0.03	CC1	1.55	Field	…	…
J21363852+3927206	−212.30 ± 0.25	−158.28 ± 0.30	20.71 ± 0.08	CC1	1.09	Field	…	…
J21374019+0137137	80.3 ± 2.8[b]	−59.4 ± 3.1[b]	…	CC1	0.42	β Pic	β Pic	Sch12b, Sch12a, Sch12c, Sh17
J21411161–1011001	−0.91 ± 1.15	−74.24 ± 1.27	62.53 ± 2.78	CC1	1.02	Field	…	…
J21501406+0922295	201.51 ± 0.07	−295.38 ± 0.08	44.36 ± 0.11	CC1	1.51	Field	…	…
J21512893–0238147	30.45 ± 0.09	−34.47 ± 0.09	46.23 ± 0.11	CC1	1.43	Field	…	…
J21521039+0537356	109.8 ± 1.5[b]	−150.0 ± 2.0[b]	…	CC1	0.64	AB Dor	AB Dor	To08, DaS09, Shk12, Ma13
J21543507+5445122	171.35 ± 0.05	142.35 ± 0.05	71.25 ± 0.16	CC1	3.19	Field	…	…
J21552437+5938371	113.0 ± 2.2[b]	22.5 ± 1.8[b]	…	CC1	0.36	Field	β Pic?	Sch12a
J22073842–0650034	146.34 ± 0.35	−2.57 ± 0.32	63.98 ± 0.80	CC1	0.95	Field	…	…
J22300418+4851347	−73.66 ± 0.10	−61.55 ± 0.09	33.26 ± 0.07	CC1	2.32	Field	…	…
J22413501+1849277	256.83 ± 1.00	95.46 ± 0.92	31.40 ± 0.65	CC1	0.23	Field	…	…
J22413577+2602128	−20.90 ± 0.10	59.67 ± 0.08	30.19 ± 0.05	CC1	3.70	Field	…	…
J22424884+1330532	57.15 ± 0.08	−34.62 ± 0.10	69.09 ± 0.33	CC1	2.24	Field	Col	Ma13, Ma14a
J22594127+2154070	127.97 ± 0.09	−59.09 ± 0.06	38.02 ± 0.07	CC1	2.28	Field	…	…
J23002791–2618431	116.72 ± 0.09	−159.84 ± 0.07	31.86 ± 0.05	CC1	2.27	AB Dor	AB Dor	Zu04, Ma13
J23024391+7506019	285.30 ± 0.05	22.95 ± 0.04	53.16 ± 0.07	CC1	3.73	Field	…	…
J23040837+0318214	104.94 ± 0.08	−53.34 ± 0.06	85.89 ± 0.34	CC1/CC2	2.20/3.73	Field	…	…
J23060295–1556151	124.2 ± 1.7[b]	−11.5 ± 1.7[b]	…	CC1	0.81	Field	…	…
J23062378+1236269	301.1 ± 4.4[b]	−52.6 ± 2.1[b]	…	CC1	0.46	Field	…	…
J23220944+5756296	−6.25 ± 1.79	−27.82 ± 1.87	166.06 ± 32.14	CC1	0.35	Field	…	…
J23450477+1458573	237.55 ± 0.29	−28.93 ± 0.14	71.79 ± 0.75	CC1	1.15	Field	…	…
J23473777–2316060	155.46 ± 0.24	−66.18 ± 0.26	44.87 ± 0.35	CC1	1.24	Field	…	…
J23574989+3837468	−155.61 ± 1.87	−145.25 ± 1.57	21.14 ± 0.67	CC1	0.47	Field	UMa?	Sh12
J23581366–1724338	225.77 ± 0.14	19.74 ± 0.09	33.45 ± 0.08	CC1	2.09	Car-Near	Hyades?, Arg?	Sh12, Ma13, El16
J23590042+2051387	228.92 ± 1.25	−104.85 ± 0.57	66.85 ± 3.56	CC1	0.56	Field	…	…

Notes.
[a] Proper motions and parallactic distance from *Gaia* DR2, unless otherwise noted.
[b] Proper motion from UCAC4 (Zacharias et al. 2013).
References. Bi15a—Binks et al. (2015), Bi15b—Binks & Jeffries (2015), Ber15—Bergfors et al. (2016), Bo15a—Bowler et al. (2015b), Br14—Brandt et al. (2014), DaS09—da Silva et al. (2009), El16—Elliott et al. (2016), Ga18b—Gagné et al. (2018a), Ga18c—Gagné & Faherty (2018), Ja14—Janson et al. (2014b), Ki10—Kiss et al. (2010), Kr14—Kraus et al. (2014), Ma13—Malo et al. (2013), Ma14a—Malo et al. (2014a), Me17—Messina et al. (2017), Na17—Naud et al. (2017), Pe13—Pecaut & Mamajek (2013), Ri14—Riedel et al. (2014), Ro11—Röser et al. (2011), Ro13—Rodriguez et al. (2013), Sch10—Schlieder et al. (2010), Sch12a—Schlieder et al. (2012b), Sch12b—Schlieder et al. (2012c), Sch12c— Schlieder et al. (2012a), Sh17—Shkolnik et al. (2017), Shk12—Shkolnik et al. (2012), St07—Stauffer et al. (2007), To08—Torres et al. (2008), Le09—Lépine & Simon (2009), Zu01b—Zuckerman et al. (2001a), Zu04—Zuckerman et al. (2004), Zu06—Zuckerman et al. (2006).
(This table is available in its entirety in machine-readable form.)

is only 1.3σ (2.3 ± 1.7 km s^{-1}) from the locus of β Pic members from Torres et al. (2008).[14] Given the excellent agreement of this system with other established β Pic members, we adopt previous membership assessments in this group over BANYAN's field hypothesis.

2MASS J00501752+0837341—This M5 star was proposed as a β Pic member by Shkolnik et al. (2017), who also identified it as an SB2, but the best hypothesis from BANYAN-Σ is the field. We measure a lithium EW of ≈60 mÅ and strong Hα emission. Using the measured RV of 2.15 ± 2.0 km s^{-1} from Shkolnik et al. (2017) together with *Gaia* DR2 astrometry, the

[14] Differential velocities (Δv) and uncertainties ($\sigma_{\Delta v}$) are calculated as follows: $\Delta v = \sqrt{(U-U_0)^2 + (V-V_0)^2 + (W-W_0)^2}$, $\sigma_{\Delta v} = \sqrt{(U-U_0)^2(\sigma_U^2 + \sigma_{U_0}^2) + (V-V_0)^2(\sigma_V^2 + \sigma_{V_0}^2) + (W-W_0)^2(\sigma_W^2 + \sigma_{W_0}^2)} / \Delta v$.

space velocities of this system are $U = -12.7 \pm 0.6$ km s^{-1}, $V = -16.6 \pm 1.0$ km s^{-1}, and $W = -7.8 \pm 1.6$ km s^{-1}. This is 1.5σ (3.0 ± 2.0 km s^{-1}) from the locus of β Pic members from Torres et al. (2008). Given the good agreement with known members, we adopt the previous membership assessment in β Pic over BANYAN's field hypothesis.

2MASS J01540267–4040440—This K7 star was proposed as a Columba member by Malo et al. (2014a), but the best hypothesis from BANYAN-Σ is the field. We measure lithium absorption with a depth of ≈160 mÅ from our SOAR/Goodman data. Using the measured RV of 12.7 ± 0.2 km s^{-1} from Malo et al. (2014a) together with *Gaia* DR2 astrometry, the space velocities of this system are $U = -11.42 \pm 0.03$ km s^{-1}, $V = -21.6 \pm 0.08$ km s^{-1}, and $W = -5.8 \pm 0.19$ km s^{-1}. This is 1.4σ (1.8 ± 1.3 km s^{-1}) from the locus of Columba members from Torres et al. (2008). Given the good kinematic agreement with Columba and appropriate lithium strength for the age of this group, we adopt the previous membership assessment in Columba over BANYAN's field hypothesis.

2MASS J02490228–1029220—Bergfors et al. (2016) identified lithium in this resolved triple system (Janson et al. 2012) and found that its kinematics are a good match to β Pic, but the best hypothesis from our BANYAN-Σ analysis is the field. We detect lithium from our SOAR spectrum with a strength of ≈310 mÅ, comparable to what Bergfors et al. measured. RVs for this system are presented in Durkan et al. (2018) and support candidacy in β Pic, although a parallax is needed to unambiguously confirm membership. We adopt previous assessments of this system as a candidate in β Pic over BANYAN's field hypothesis.

2MASS J03520223+2439479—This star is a known member of the Pleiades (e.g., Stauffer et al. 2007). It has also been proposed as a member of Taurus, but Kraus et al. (2017) showed that its proper motion is inconsistent with that region. Walter et al. (1988) and Soderblom et al. (1993) measured lithium equivalent widths of 350 and 302 mÅ, respectively. The $0\farcs45$ binary companion we uncovered with Robo-AO was first reported by Leinert et al. (1993). *Gaia* DR2 reported a parallax of 2.2 ± 0.7 mas (≈450 pc), but the astrometric excess noise parameter is large (2.5 mas), implying the five-parameter astrometric solution is not an especially good fit to the data. This is likely caused by acceleration from the binary companion so the reported parallax is probably unreliable. We adopt previous assessments of this system as a member of the Pleiades over BANYAN's field hypothesis.

2MASS J04435686+3723033—Schlieder et al. (2010) identified this object and its wide (≈9″) comoving companion as likely members of the β Pic moving group based on their activity and proper motions from SUPERBLINK. β Pic membership is reaffirmed in Malo et al. (2014b), Messina et al. (2017), and Shkolnik et al. (2017), but the best hypothesis from our BANYAN-Σ analysis is the field. Together with the *Gaia* distance of 71.65 ± 0.26 pc and RV of -6.4 ± 0.2 km s^{-1} from Malo et al. (2014b), these proper motions imply *UVW* space velocities of -10.66 ± 0.19 km s^{-1}, -19.08 ± 0.09 km s^{-1}, and -8.40 ± 0.05 km s^{-1}. These differ by 3.7σ (3.3 km $\pm$ 0.9 km s^{-1}) from the locus of β Pic from Torres et al. (2008). The M2 host star shows modest lithium absorption (194 ± 4 mÅ from Malo et al. 2014b and ≈120 mÅ from our Mayall spectrum), consistent with an age older than TWA but younger than Tuc-Hor. We adopt previous assessments of this system as a candidate member of β Pic over BANYAN's field hypothesis.

2MASS J05363633+2139330—Li & Hu (1998) first identified this star as a candidate member of Taurus from its activity and strong lithium absorption (480 mÅ). We also detect deep lithium in this star with an EW of ≈460 mÅ, but found a spectral type of M2, which differs from the K4 classification by Li & Hu (1998). Mamajek (2016a) suggested that this star is a member of the proposed subgroup 118 Tau, which is also suggested as the best hypothesis from BANYAN-Σ. Membership in the broader Taurus complex was recently confirmed by a detailed analysis by Kraus et al. (2017); they also find this subgroup may be kinematically related to Taurus. The proper motion and distance for this star from *Gaia* DR2 is $\mu_\alpha \cos\delta = 10.65 \pm 0.19$ mas yr^{-1}, $\mu_\delta = -41.23 \pm 0.14$ mas yr^{-1}, and 108.22 ± 1.59 pc, respectively, similar to the other 118 Tau group members from Mamajek (2016a) ($\mu_\alpha \cos\delta \approx +4$ mas yr^{-1}; $\mu_\delta \approx -39$ mas yr^{-1}; $d \approx 120$ pc). Given this consistent sky position, proper motion, and distance, we adopt candidacy in 118 Tau as suggested by Mamajek (2016a) and BANYAN.

2MASS J05374649+0231264—da Silva et al. (2009) first identified this lithium-rich (EW = 300 mÅ) star as a member of Columba, which was bolstered by Elliott et al. (2016). We measure a somewhat lower lithium strength of ≈190 mÅ from our low-resolution Mayall spectrum. Using the proper motion, distance (68.44 ± 0.19 pc), and RV (20.8 ± 2.8 km s^{-1}) from *Gaia* DR2, the space velocities of this system are $U = -13.1 \pm 2.5$ km s^{-1}, $V = -20.6 \pm 1.0$ km s^{-1}, and $W = -6.5 \pm 0.7$ km s^{-1}. This is 1.0σ (1.3 ± 1.3 km s^{-1}) from the locus of Columba members from Torres et al. (2008). Given the good kinematic agreement with Columba and appropriate lithium strength for the age of this group, we adopt previous membership assessment in Columba over BANYAN's field hypothesis.

2MASS J05500858+0511536—We measure modest lithium (≈120 mÅ) in this little-studied active M2 star. The best hypothesis from BANYAN-Σ is Columba. Using the proper motion, distance (64.45 ± 0.17 pc), and RV (18 ± 4 km s^{-1}) from *Gaia* DR2, the space velocities of this system are $U = -11.2 \pm 3.7$ km s^{-1}, $V = -19.2 \pm 1.4$ km s^{-1}, and $W = -5.2 \pm 0.8$ km s^{-1}. This is 1.3σ (3.3 ± 2.7 km s^{-1}) from the locus of Columba members from Torres et al. (2008). The absolute *V*-band magnitude of 8.6 mag and *V* – *J* color of 3.3 mag place this star above the main sequence, in good agreement with other Columba members from Bell et al. (2015). Overall, this star appears to be an excellent new candidate member of Columba, but a more precise RV and lithium equivalent width measurement is needed for confirmation.

2MASS J09595765–7221472—Elliott et al. (2014) identified this lithium-rich star as a K4 candidate member of Carina, but the best hypothesis from BANYAN-Σ is the field. We find a somewhat later spectral type of K7 from our SOAR spectra. Our lithium measurement (EW ≈ 270 mÅ) is comparable to that of Torres et al. (2006; EW = 330 mÅ) and suggests an age between TWA and AB Dor (e.g., Murphy et al. 2018). The velocities of this system are $U = -8.8 \pm 0.07$ km s^{-1}, $V = -21.6 \pm 0.18$ km s^{-1}, and $W = -2.1 \pm 0.05$ km s^{-1}. This is 2.5σ (3.0 ± 1.2 km s^{-1}) from the locus of Carina members from Torres et al. (2008). This star is a better match to Tuc-Hor in terms of space motion, but is several tens of parsecs from established members of that group. We adopt previous assessments of this system as a member of Carina over BANYAN's field hypothesis.

2MASS J10260210–4105537—This lithium-rich early-M dwarf was proposed as a member of TWA by Bell et al. (2015), Pecaut & Mamajek (2013), and Naud et al. (2017). Gagné et al. (2017) suggested that it is a likely contaminant from Lower Centaurus Crux (LCC). Using the new *Gaia* DR2 distance of 84.9 ± 2 pc, the best hypothesis from BANYAN-Σ is the field. We measure a spectral type of M2 and strong lithium (EW ≈ 410 mÅ), which is slightly less than that found by Rodriguez et al. (2011; EW = 500 ± 70 mÅ). We also find unusually strong Hα (EW ≈ −10.4 Å) above the envelope of saturated chromospheric emission identified by Barrado y Navascués & Martin (2003), suggesting it may originate from ongoing accretion. The distance and sky position of this object are more consistent with TWA than LCC (e.g., Murphy et al. 2015), so we adopt previous assessments of this system as a likely member of TWA over LCC and BANYAN's field hypothesis. However, a radial velocity is needed to unambiguously establish group membership.

2MASS J12003688–6337055—This active, lithium-rich (EW ≈ 480 mÅ) M0 star was flagged as a likely LCC member using BANYAN-Σ. Using the proper motion, distance (101.2 ± 0.3 pc), and RV (14.3 ± 1.8 km s^{-1}) from *Gaia* DR2, the space velocities of this system are $U = -9.7 \pm 0.8$ km s^{-1}, $V = -21.06 \pm 1.6$ km s^{-1}, and $W = -8.02 \pm 0.06$ km s^{-1}. This is 1.1σ (2.7 ± 2.5 km s^{-1}) from the locus of LCC members from Gagné et al. (2018b). The *V*-band absolute magnitude of this star is 7.0 mag, which is about a magnitude above the main sequence at the $V - J$ color of this object (2.7 mag; Bell et al. 2015). The sky position, space motion, lithium strength, and overluminosity are in excellent agreement with LCC.

2MASS J12281909–7306346—This active M0 star has strong lithium absorption—EW ≈ 440 mÅ from our low-resolution Goodman spectrum—and has a best hypothesis of ϵ Cha from BANYAN-Σ. It does not appear to be a previously known young star. The space velocities of this system from *Gaia* DR2 astrometry are $U = -8.5 \pm 0.7$ km s^{-1}, $V = -21.0 \pm 1.0$ km s^{-1}, and $W = -7.9 \pm 0.3$ km s^{-1}. This is 2.4σ (3.7 ± 1.5 km s^{-1}) from the locus of ϵ Cha members from Gagné et al. (2018b). We also note that this star's kinematics and distance (107 ± 2 pc) line up well with the locus of LCC members (0.9σ, or 1.9 ± 2.2 km s^{-1}). Its sky position is just beyond the canonical (albeit arbitrarily defined) southern boundary of LCC at $b = -10°$, but all other indicators agree well with that association. We conclude that this star could plausibly belong to ϵ Cha or LCC, though the extended LCC is a better kinematic match.

2MASS J12445897–6026409—This M1 star was identified as a potential member of LCC using BANYAN-Σ. We measure strong lithium absorption (EW ≈ 340 mÅ) consistent with LCC members of this spectral type. The space velocities of this system from *Gaia* DR2 astrometry are $U = -6.7 \pm 0.4$ km s^{-1}, $V = -18.3 \pm 0.3$ km s^{-1}, and $W = -4.5 \pm 0.3$ km s^{-1}. This is 1.1σ (3.8 ± 3.4 km s^{-1}) from the locus of LCC members from Gagné et al. (2018b). We conclude that this star is a previously unrecognized member of LCC.

2MASS J13314666+2916368—We measure unusually strong Hα emission of −16.2 Å from this M5 star, suggesting it may originate from ongoing accretion. The parallactic distance from *Gaia* is 18.3 pc. Riedel et al. (2014) identified this close binary as a possible member of Carina or Columba. If it is a member of either of these groups and if the strong Hα originates from ongoing accretion, this would be an unusually long disk dissipation timescale possibly similar to the peculiar system found by Murphy et al. (2018).

2MASS J13493313–6818291—Malo et al. (2013) identified this active M dwarf as a candidate member of Argus, but we find that the best hypothesis from BANYAN-Σ is LCC. Janson et al. (2012) resolved it into a close visual triple. We measure a spectral type of M3 and find strong lithium (EW ≈ 360 mÅ) from our moderate-resolution Goodman spectrum, implying an age significantly younger than Argus (≈40–50 Myr; Zuckerman 2019). The distance (99.8 ± 1.5 pc) and proper motion ($\mu_\alpha \cos\delta = -31.1 \pm 0.2$ mas yr^{-1}, $\mu_\delta = -19.7 \pm 0.2$ mas yr^{-1}) are in good agreement with LCC. We conclude that this star is most likely an LCC member, but an RV is needed for confirmation.

2MASS J15354856–2958551—This M4 star is noteworthy for having the strongest Hα emission (EW ≈ −43 Å) of any star for which we obtained a spectrum in this program, indicating active disk accretion. Brandner et al. (1996) resolved this star into a 0$''$9 binary and Barenfeld et al. (2016) detected the disk in continuum and CO line emission with ALMA. Köhler et al. (2000) identified this star as a member of USco, but our BANYAN-Σ analysis suggests it is a field star based on the UCAC4 proper motion (no astrometric solution is presented in *Gaia* DR2). We measure strong lithium with an EW of ≈500 mÅ, implying a young age consistent with members of the Sco-Cen complex and certainly less than a few tens of 10 Myr. We note that the sky position and proper motion align with UCL. We conclude that this star is a good candidate for UCL, but an RV and parallax are needed to fully assess membership in this subgroup.

2MASS J15451903–4431361—This little-studied active M3 star shows strong lithium absorption (EW ≈ 380 mÅ) and was identified as a candidate UCL member using BANYAN-Σ. The sky position and proper motion are in good agreement with UCL members, but the distance from *Gaia* DR2 of 89.3 ± 3.7 pc is much closer than the vast majority of established members (Wright & Mamajek 2018). However, this does not exclude candidacy in that subgroup because our targets are intentionally biased to closer distances, which would naturally sample the closest members of this complex. We also note that the *Gaia* DR2 excess noise parameter for this target is quite large (3.1 mas), which may point to an unseen companion that could be affecting the five-parameter astrometric fit. We conclude that this star may be an unusually nearby member of UCL, but an RV (and perhaps better parallax solution) is needed for confirmation.

2MASS J16430128–1754274—This active M1 star has been widely listed as a kinematic member of β Pic (e.g., Kiss et al. 2010; Binks & Jeffries 2014; Shkolnik et al. 2017). However, the best hypothesis from BANYAN-Σ is the field, and it received a low membership probability in β Pic in Malo et al. (2013). This star has strong lithium absorption, with EW measurements of 300 ± 20 mÅ by Kiss et al. (2010), 364 ± 20 mÅ by Binks & Jeffries (2014), and ≈280 mÅ in this work from our low-resolution RC-Spec spectrum. Based on the *Gaia* DR2 distance of 71.1 ± 0.3 pc and RV of −9.3 ± 0.4 km s^{-1} from Malo et al. (2014a), the space velocities of this system are $U = -7.6 \pm 0.4$ km s^{-1},

$V = -20.1 \pm 0.08$ km s^{-1}, and $W = -5.7 \pm 0.13$ km s^{-1}. This is 5.0σ (6.0 ± 1.2 km s^{-1}) from the locus of β Pic members from Torres et al. (2008). We conclude that this star is a poor match with β Pic and does not agree especially well with any other known nearby moving groups.

2MASS J16455062+0343014—Schlieder et al. (2012b, 2012c) identified this active M dwarf as a likely member of AB Dor, but the best hypothesis from BANYAN-Σ is the field. We measure a spectral type of M2 and find modest lithium absorption (EW $\approx$ 120 mÅ). We also resolve this source into a 2$''$ binary with Robo-AO and confirm that the pair are physically bound. Based on the *Gaia* DR2 distance of 44.89 ± 0.08 pc and RV of -15.5 ± 0.7 km s^{-1} from Schlieder et al. (2012c), the space velocities of this system are $U = -2.3 \pm 0.6$ km s^{-1}, $V = -26.3 \pm 0.2$ km s^{-1}, and $W = -11.2 \pm 0.3$ km s^{-1}. This is 3.4σ (5.0 ± 1.5 km s^{-1}) from the locus of AB Dor members from Torres et al. (2008). However, when we use the RV of -21.7 ± 1.8 km s^{-1} from *Gaia* DR2, the space velocities of this system are $U = -7.4 \pm 1.4$ km s^{-1}, $V = -28.2 \pm 0.6$ km s^{-1}, and $W = -14.2 \pm 0.9$ km s^{-1}, or only 0.9σ (1.5 ± 1.6 km s^{-1}) from the locus of AB Dor members. We conclude that this visual and spectroscopic binary remains an excellent candidate member of AB Dor. Longer baseline RV monitoring will be useful to measure a systemic velocity for this pair.

2MASS J17213497–2152283—We measure strong Hα emission (EW ≈ -13.4 Å) and lithium absorption (EW $\approx$ 370 mÅ) in this little-studied active M4 star. The best hypothesis from BANYAN-Σ is UCL, but the sky position lies at the eastern edge of USco and disagrees with the UCL subgroup. However, the distance from *Gaia* DR2 of 101.0 ± 0.7 pc places it closer than nearly all USco members (Wright & Mamajek 2018). We conclude that this star is likely related to the Sco-Cen complex, but perhaps not directly associated with the canonically defined subgroups.

2MASS J23093711–0225551—This active K4 star was identified as a candidate member of Carina by Elliott et al. (2014) but the best hypothesis from BANYAN-Σ is the field. Based on parallactic distance of 52.6 ± 0.4 pc and RV of -12.7 ± 0.4 km s^{-1} from *Gaia* DR2, the space velocities of this star are $U = -9.64 \pm 0.09$ km s^{-1}, $V = -20.8 \pm 0.2$ km s^{-1}, and $W = -0.2 \pm 0.3$ km s^{-1}. This is 3.4σ (4.7 ± 1.4 km s^{-1}) from the locus of Carina members from Torres et al. (2008). The kinematics are in good agreement with Tuc-Hor, but this star would be a spatial outlier if it belongs to that group. We measure weak lithium (EW $\approx$ 130 mÅ) from our low-resolution Goodman spectrum, implying an age older than β Pic but consistent with scatter in Tuc-Hor and AB Dor. We conclude that this star is most consistent with the field, but could be a kinematic outlier of Carina or perhaps a spatial outlier of Tuc-Hor.

6. Summary

The goal of this study is to identify new young stars in the solar neighborhood for future direct imaging surveys of exoplanets. We began with a sample of 2060 late-K through early-M dwarfs selected on the basis of X-ray and UV activity cuts, proper motions, NIR color cuts, and optical brightness. Follow-up low-resolution optical spectra were obtained for 632 stars, 58 of which show strong lithium absorption. Among the lithium-rich stars, 34 are previously known members of nearby moving groups while seven are new. The rest appear to be young field stars without any obvious connection to an established kinematic group. We also acquired Robo-AO observations of 1011 northern stars in our sample of active K/M dwarfs; 239 of these have nearby point sources within 4$''$, the majority of which are likely to be physical companions. Many of these have kinematics consistent with YMGs, which long-baseline RV monitoring can better constrain by measuring systemic RVs.

It is a pleasure to thank Diane Harmer, Sean Points, and all support staff and telescope operators at KPNO and CTIO who helped make these observations possible. C.Z. is supported by a Dunlap Fellowship at the Dunlap Institute for Astronomy & Astrophysics, funded through an endowment established by the Dunlap family and the University of Toronto. V.S. was supported part from the John W. Cox Endowment for the Advanced Studies in Astronomy. This publication makes use of data products from the Two Micron All Sky Survey, which is a joint project of the University of Massachusetts and the Infrared Processing and Analysis Center/California Institute of Technology, funded by the National Aeronautics and Space Administration and the National Science Foundation. This work has made use of data from the European Space Agency (ESA) mission *Gaia* (https://www.cosmos.esa.int/gaia), processed by the *Gaia* Data Processing and Analysis Consortium (DPAC; https://www.cosmos.esa.int/web/gaia/dpac/consortium). Funding for the DPAC has been provided by national institutions, in particular the institutions participating in the *Gaia* Multilateral Agreement. This publication makes use of data products from the *Wide-field Infrared Survey Explorer*, which is a joint project of the University of California, Los Angeles, and the Jet Propulsion Laboratory/California Institute of Technology, funded by the National Aeronautics and Space Administration. The Robo-AO system was developed by collaborating partner institutions, the California Institute of Technology and the Inter-University Centre for Astronomy and Astrophysics, and with the support of the National Science Foundation under grant Nos. AST-0906060, AST-0960343, and AST-1207891; the Mt. Cuba Astronomical Foundation; and by a gift from Samuel Oschin. Ongoing science operation support of Robo-AO is provided by the California Institute of Technology and the University of Hawai'i. C.B. acknowledges support from the Alfred P. Sloan Foundation. NASA's Astrophysics Data System Bibliographic Services together with the VizieR catalog access tool and SIMBAD database operated at CDS, Strasbourg, France, were invaluable resources for this work. Based on observations made with the NASA *Galaxy Evolution Explorer*. *GALEX* is operated for NASA by the California Institute of Technology under NASA contract NAS5-98034. This research has made use of the Washington Double Star Catalog maintained at the U.S. Naval Observatory.

Based in part on observations obtained at the Southern Astrophysical Research (SOAR) telescope (NOAO Prop. ID 2013B-0496, 2014A-0019, 2015A-0016; PI: B. Bowler), which is a joint project of the Ministério da Ciência, Tecnologia, Inovaçãos e Comunicaçãoes (MCTIC) do Brasil, the U.S. National Optical Astronomy Observatory (NOAO), the University of North Carolina at Chapel Hill (UNC), and Michigan State University (MSU). Based in part on observations at Kitt Peak National Observatory, National Optical Astronomy Observatory (NOAO Prop. IDs 2013B-0496, 2014A-0019, 2015A-0016; PI: B. Bowler), which is operated by the Association of Universities for Research in Astronomy (AURA) under cooperative agreement with the National Science Foundation. Institutional allocation for the Robo-AO observations at the P60 telescope was provided based on the prior affiliation of B.P.B. and S.H. with the California Institute of Technology. The authors are honored to be permitted to conduct astronomical research on Iolkam Du'ag (Kitt Peak), a mountain with particular significance to the Tohono O'odham.

Facilities: Mayall (RC-Spec), SOAR (Goodman Spectrograph), PO:1.5 m (Robo-AO), UH:2.2 m (SNIFS).

ORCID iDs

Brendan P. Bowler https://orcid.org/0000-0003-2649-2288
Sasha Hinkley https://orcid.org/0000-0001-8074-2562
Carl Ziegler https://orcid.org/0000-0002-0619-7639
Christoph Baranec https://orcid.org/0000-0002-1917-9157
John E. Gizis https://orcid.org/0000-0002-8916-1972
Nicholas M. Law https://orcid.org/0000-0001-9380-6457
Michael C. Liu https://orcid.org/0000-0003-2232-7664
Evgenya L. Shkolnik https://orcid.org/0000-0002-7260-5821
Basmah Riaz https://orcid.org/0000-0003-3863-4052
Reed Riddle https://orcid.org/0000-0002-0387-370X

References

Aldering, G., Antilogus, P., Bailey, S., et al. 2006, ApJ, 650, 510
Aller, K. M., Liu, M. C., Magnier, E. A., et al. 2016, ApJ, 821, 120
Allers, K. N., & Liu, M. C. 2013, ApJ, 772, 79
Anderson, E., & Francis, C. 2012, AstL, 38, 331
Ansdell, M., Gaidos, E., Mann, A. W., et al. 2015, ApJ, 798, 41
Baranec, C., Riddle, R., Law, N. M., et al. 2013, JVE, 72, e50021
Baranec, C., Riddle, R., Law, N. M., et al. 2014, ApJL, 790, L8
Barenfeld, S. A., Carpenter, J. M., Ricci, L., & Isella, A. 2016, ApJ, 827, 142
Barrado y Navascués, D., & Martin, E. L. 2003, AJ, 126, 2997
Basri, G., Marcy, G. W., & Graham, J. R. 1996, ApJ, 458, 600
Bell, C. P. M., Mamajek, E. E., & Naylor, T. 2015, MNRAS, 454, 593
Bergfors, C., Brandner, W., Bonnefoy, M., et al. 2016, MNRAS, 456, 2576
Bergfors, C., Brandner, W., Janson, M., et al. 2010, A&A, 520, A54
Best, W. M. J., Liu, M. C., Dupuy, T. J., & Magnier, E. A. 2017, ApJL, 843, L4
Beuzit, J.-L., Ségransan, D., Forveille, T., et al. 2004, A&A, 425, 997
Bildsten, L., Brown, E. F., Matzner, C. D., & Ushomirsky, G. 1997, ApJ, 482, 442
Biller, B. A., Liu, M. C., Wahhaj, Z., et al. 2013, ApJ, 777, 160
Binks, A. S., & Jeffries, R. D. 2014, MNRAS, 438, L11
Binks, A. S., & Jeffries, R. D. 2015, MNRAS, 455, 3345
Binks, A. S., Jeffries, R. D., & Maxted, P. F. L. 2015, MNRAS, 452, 173
Bowler, B. P. 2016, PASP, 128, 102001
Bowler, B. P., Liu, M. C., Mawet, D., et al. 2017, AJ, 153, 1
Bowler, B. P., Liu, M. C., Shkolnik, E. L., & Dupuy, T. J. 2013, ApJ, 774, 55
Bowler, B. P., Liu, M. C., Shkolnik, E. L., & Tamura, M. 2015a, ApJS, 216, 7
Bowler, B. P., & Nielsen, E. L. 2018, in Handbook of Exoplanets, ed. H. Deeg & J. Belmonte (Cham: Springer International), 155
Bowler, B. P., Shkolnik, E. L., Liu, M. C., et al. 2015b, ApJ, 806, 62
Brandner, W., Alcalá, J. M., Kunkel, M., Moneti, A., & Zinnecker, H. 1996, A&A, 307, 121
Brandt, T. D., Kuzuhara, M., McElwain, M. W., et al. 2014, ApJ, 786, 1
Chabrier, G., Baraffe, I., & Plez, B. 1996, ApJL, 459, L91
Chauvin, G., Lagrange, A.-M., Dumas, C., et al. 2004, A&A, 425, L29
Chauvin, G., Vigan, A., Bonnefoy, M., et al. 2015, A&A, 573, A127
Clemens, J. C., Crain, J. A., & Anderson, R. 2004, Proc. SPIE, 5492, 331
Close, L. M., Lenzen, R., Guirado, J. C., et al. 2005, Natur, 433, 286
Covey, K. R., Ivezić, Ž., Schlegel, D., et al. 2007, AJ, 134, 2398
Cutri, R. M., Skrutskie, M. F., Van Dyk, S., et al. 2003, The IRSA 2MASS All-Sky Point Source Catalog, NASA/IPAC Infrared Science Archive, http://irsa.ipac.caltech.edu/applications/Gator/
Daemgen, S., Siegler, N., Reid, I. N., & Close, L. M. 2007, ApJ, 654, 558
Delfosse, X., Forveille, T., Beuzit, J.-L., et al. 1999, A&A, 344, 897
Desidera, S., Covino, E., Messina, S., et al. 2015, A&A, 573, A126
da Silva, L., Torres, C. A. O., De La Reza, R., et al. 2009, A&A, 508, 833
Durkan, S., Janson, M., Ciceri, S., et al. 2018, A&A, 618, A5
Elliott, P., Bayo, A., Melo, C. H. F., et al. 2014, A&A, 568, A26
Elliott, P., Bayo, A., Melo, C. H. F., et al. 2016, A&A, 590, A13
Elliott, P., Huélamo, N., Bouy, H., et al. 2015, A&A, 580, A88
Evans, D. W., Irwin, M. J., & Helmer, L. 2002, A&A, 395, 347
Faherty, J. K., Riedel, A. R., Cruz, K. L., et al. 2016, ApJS, 225, 10
Filippenko, A. V. 1982, PASP, 94, 715
Frith, J., Pinfield, D. J., Jones, H. R. A., et al. 2013, MNRAS, 435, 2161
Gagné, J., & Faherty, J. K. 2018, ApJ, 862, 138
Gagné, J., Faherty, J. K., Cruz, K. L., et al. 2015, ApJS, 219, 33
Gagné, J., Faherty, J. K., & Fontaine, G. 2018a, RNAAS, 2, 9
Gagné, J., Faherty, J. K., Mamajek, E. E., et al. 2017, ApJS, 228, 18
Gagné, J., LaFreniere, D., Doyon, R., Malo, L., & Artigau, E. 2014, ApJ, 783, 121
Gagné, J., Mamajek, E. E., Malo, L., et al. 2018b, ApJ, 856, 23
Gaia Collaboration, Brown, A. G. A., Vallenari, A., et al. 2018, A&A, 616, A1
Gaidos, E., Mann, A. W., Lépine, S., et al. 2014, MNRAS, 443, 2561
Gizis, J. E. 2002, ApJ, 575, 484
Goldman, B., Röser, S., Schilbach, E., Moór, A. C., & Henning, T. 2018, ApJ, 868, 32
Guenther, E. W., Paulson, D. B., Cochran, W. D., et al. 2005, A&A, 442, 1031
Haakonsen, C. B., & Rutledge, R. E. 2009, ApJS, 184, 138
Hamuy, M., Suntzeff, N. B., Heathcote, S. R., et al. 1994, PASP, 106, 566
Hamuy, M., Walker, A. R., Suntzeff, N. B., et al. 1992, PASP, 104, 533
Horne, K. 1986, PASP, 98, 609
Janson, M., Bergfors, C., Brandner, W., et al. 2014a, ApJ, 789, 102
Janson, M., Bergfors, C., Brandner, W., et al. 2014b, ApJS, 214, 17
Janson, M., Durkan, S., Bonnefoy, M., et al. 2018, A&A, 620, A33
Janson, M., Durkan, S., Hippler, S., et al. 2017, A&A, 599, A70
Janson, M., Hormuth, F., Bergfors, C., et al. 2012, ApJ, 754, 44
Jayawardhana, R., & Brandeker, A. 2001, ApJL, 561, L111
Jodar, E., Pérez-Garrido, A., Díaz-Sánchez, A., et al. 2013, MNRAS, 429, 859
Kass, R. E., & Raftery, A. E. 1995, J. Am. Stat. Assoc., 90, 773
Kastner, J. H., Zuckerman, B., Weintraub, D. A., & Forveille, T. 1997, Sci, 277, 67
Kiss, L. L., Moór, A., Szalai, T., et al. 2010, MNRAS, 411, 117
Köhler, R., Kunkel, M., Leinert, C., & Zinnecker, H. 2000, A&A, 356, 541
Kraus, A. L., Herczeg, G. J., Rizzuto, A. C., et al. 2017, ApJ, 838, 150
Kraus, A. L., Shkolnik, E. L., Allers, K. N., & Liu, M. C. 2014, AJ, 147, 146
Lagrange, A.-M., Bonnefoy, M., Chauvin, G., et al. 2010, Sci, 329, 57
Lantz, B., Aldering, G., Antilogus, P., et al. 2004, Proc. SPIE, 5249, 146
Law, N. M., Hodgkin, S. T., & Mackay, C. D. 2008, MNRAS, 384, 150
Law, N. M., Morton, T., Baranec, C., et al. 2014, ApJ, 791, 35
Leinert, C., Zinnecker, H., Weitzel, N., et al. 1993, A&A, 278, 129
Lépine, S., & Gaidos, E. 2011, AJ, 142, 138
Lépine, S., & Simon, M. 2009, AJ, 137, 3632
Li, J. Z., & Hu, J. Y. 1998, A&AS, 132, 173
Lindegren, L., Hernández, J., Bombrun, A., et al. 2018, A&A, 616, A2
Liu, M. C., Dupuy, T. J., & Allers, K. N. 2016, ApJ, 833, 1
Liu, M. C., Magnier, E. A., Deacon, N. R., et al. 2013, ApJL, 777, L20
López Martí, B., Jimenez Esteban, F., Bayo, A., et al. 2013, A&A, 551, A46
Macintosh, B., Graham, J. R., Barman, T., et al. 2015, Sci, 350, 64
Malo, L., Artigau, E., Doyon, R., et al. 2014a, ApJ, 788, 81
Malo, L., Doyon, R., Feiden, G. A., et al. 2014b, ApJ, 792, 37
Malo, L., Doyon, R., Lafrenière, D., et al. 2013, ApJ, 762, 88
Mamajek, E. 2016a, figshare, 3122689, https://figshare.com/articles/A_New_Candidate_Young_Stellar_Group_at_d_121_pc_Associated_with_118_Tauri/3122689
Mamajek, E. E. 2016b, in IAU Symp. 314, Young Stars & Planets Near the Sun (Cambridge: Cambridge Univ. Press), 21
Mamajek, E. E., Lawson, W. A., & Feigelson, E. D. 1999, ApJL, 516, L77
Markwardt, C. B. 2009, in ASP Conf. Ser. 411, Astronomical Data Analysis Software and Systems XVIII, ed. D. A. Bohlender, D. Durand, & P. Dowler (San Francisco, CA: ASP), 251
Marois, C., Macintosh, B., Barman, T., et al. 2008, Sci, 322, 1348
Martin, D. C., Fanson, J., Schiminovich, D., et al. 2005, ApJL, 619, L1
Mason, B. D., Wycoff, G. L., Hartkopf, W. I., Douglass, G. G., & Worley, C. E. 2001, AJ, 122, 3466
McCarthy, C., Zuckerman, B., & Becklin, E. E. 2001, AJ, 121, 3259
Mentuch, E., Brandeker, A., van Kerkwijk, M. H., Jayawardhana, R., & Hauschildt, P. H. 2008, ApJ, 689, 1127
Messina, S., Lanzafame, A. C., Malo, L., et al. 2017, A&A, 607, A3
Monet, D. G., Levine, S. E., Canzian, B., et al. 2003, AJ, 125, 984
Montet, B. T., Bowler, B. P., Shkolnik, E. L., et al. 2015, ApJL, 813, L11
Morrissey, P., Conrow, T., Barlow, T. A., et al. 2007, ApJS, 173, 682
Murphy, S. J., Lawson, W. A., & Bento, J. 2015, MNRAS, 453, 2220
Murphy, S. J., Lawson, W. A., & Bessell, M. S. 2013, MNRAS, 435, 1325
Murphy, S. J., Mamajek, E. E., & Bell, C. P. M. 2018, MNRAS, 476, 3290
Naud, M.-E., Artigau, E., Doyon, R., et al. 2017, AJ, 154, 129
Naud, M.-E., Artigau, E., Malo, L., et al. 2014, ApJ, 787, 5
Neuhäuser, R. 1997, Sci, 276, 1363

Nguyen, D. C., Brandeker, A., van Kerkwijk, M. H., & Jayawardhana, R. 2012, ApJ, 745, 119
Nielsen, E. L., De Rosa, R. J., Wang, J., et al. 2016, AJ, 152, 175
Oke, J. B. 1990, AJ, 99, 1621
Pecaut, M. J., & Mamajek, E. E. 2013, ApJS, 208, 9
Pecaut, M. J., & Mamajek, E. E. 2016, MNRAS, 461, 794
Reid, I. N., Hawley, S. L., & Gizis, J. E. 1995, AJ, 110, 1838
Riaz, B., Gizis, J. E., & Harvin, J. 2006, AJ, 132, 866
Riddle, R. L., Hogstrom, K., Papadopoulos, A., Baranec, C., & Law, N. M. 2014, Proc. SPIE, 9152, 91521E
Riedel, A. R., Alam, M. K., Rice, E. L., Cruz, K. L., & Henry, T. J. 2017, ApJ, 840, 87
Riedel, A. R., Finch, C. T., Henry, T. J., et al. 2014, AJ, 147, 85
Rodriguez, D. R., Bessell, M. S., Zuckerman, B., & Kastner, J. H. 2011, ApJ, 727, 62
Rodriguez, D. R., Zuckerman, B., Kastner, J. H., et al. 2013, ApJ, 774, 101
Roeser, S., Demleitner, M., & Schilbach, E. 2010, AJ, 139, 2440
Röser, S., Schilbach, E., Piskunov, A. E., Kharchenko, N. V., & Scholz, R.-D. 2011, A&A, 531, A92
Scalzo, R. A., Aldering, G., Antilogus, P., et al. 2010, ApJ, 713, 1073
Schlieder, J. E., Lépine, S., Rice, E., et al. 2012a, AJ, 143, 114
Schlieder, J. E., Lépine, S., & Simon, M. 2010, AJ, 140, 119
Schlieder, J. E., Lépine, S., & Simon, M. 2012b, AJ, 143, 80
Schlieder, J. E., Lépine, S., & Simon, M. 2012c, AJ, 144, 109
Schneider, G., Hershey, J. L., & Wenz, M. T. 1998, PASP, 110, 1012
Schwarz, G. 1978, AnSta, 6, 461
Shan, Y., Yee, J. C., Bowler, B. P., et al. 2017, ApJ, 846, 93
Shkolnik, E., Liu, M. C., & Reid, I. N. 2009, ApJ, 699, 649
Shkolnik, E. L., Allers, K. N., Kraus, A. L., Liu, M. C., & Flagg, L. 2017, AJ, 154, 69
Shkolnik, E. L., Anglada-Escudé, G., Liu, M. C., et al. 2012, ApJ, 758, 56
Shkolnik, E. L., & Barman, T. S. 2014, AJ, 148, 64
Shkolnik, E. L., Liu, M. C., Reid, I. N., Dupuy, T., & Weinberger, A. J. 2011, ApJ, 727, 6
Silvestri, N. M., Lemagie, M. P., Hawley, S. L., et al. 2007, AJ, 134, 741
Skrutskie, M. F., Cutri, R. M., Stiening, R., et al. 2006, AJ, 131, 1163
Slesnick, C. L., Carpenter, J. M., Hillenbrand, L. A., & Mamajek, E. E. 2006, AJ, 132, 2665
Soderblom, D. R., Hillenbrand, L. A., Jeffries, R. D., Mamajek, E. E., & Naylor, T. 2014, in Protostars and Planets VI, ed. H. Beuther et al. (Tucson, AZ: Univ. of Arizona Press), 219
Soderblom, D. R., Jones, B. F., Balachandran, S., et al. 1993, AJ, 106, 1059
Song, I., Zuckerman, B., & Bessell, M. S. 2012, AJ, 144, 8
Stauffer, J. R., Hartmann, L. W., Fazio, G. G., et al. 2007, ApJS, 172, 663
Stauffer, J. R., Schultz, G., & Kirkpatrick, J. D. 1998, ApJL, 499, L199
Torres, C. A. O., da Silva, L., Quast, G. R., de la Reza, R., & Jilinski, E. 2000, AJ, 120, 1410
Torres, C. A. O., Quast, G. R., da Silva, L., et al. 2006, A&A, 460, 695
Torres, C. A. O., Quast, G. R., Melo, C. H. F., & Sterzik, M. F. 2008, in Handbook of Star Forming Regions, Volume II: The Southern Sky, ed. B. Reipurth (San Francisco, CA: ASP), 757
Voges, W., Aschenbach, B., Boller, T., et al. 1999, A&A, 349, 389
Voges, W., Aschenbach, B., Boller, T., et al. 2000, IAUC, 7432, 3
Walter, F. M., Brown, A., Mathieu, R. D., Myers, P. C., & Vrba, F. J. 1988, AJ, 96, 297
West, A. A., Morgan, D. P., Bochanski, J. J., et al. 2011, AJ, 141, 97
White, R. J., Gabor, J. M., & Hillenbrand, L. A. 2007, AJ, 133, 2524
Wright, E. L., Eisenhardt, P. R. M., Mainzer, A. K., et al. 2010, AJ, 140, 1868
Wright, N. J., & Mamajek, E. E. 2018, MNRAS, 476, 381
Wyatt, M. C., Panic, O., Kennedy, G. M., & Matra, L. 2015, Ap&SS, 357, 103
Zacharias, N., Finch, C. T., Girard, T. M., et al. 2013, AJ, 145, 44
Ziegler, C., Law, N. M., Morton, T., et al. 2017, AJ, 153, 66
Zuckerman, B. 2019, ApJ, 870, 27
Zuckerman, B., Bessell, M. S., Song, I., & Kim, S. 2006, ApJL, 649, L115
Zuckerman, B., Song, I., & Bessell, M. S. 2004, ApJL, 613, L65
Zuckerman, B., Song, I., Bessell, M. S., & Webb, R. A. 2001a, ApJL, 562, L87
Zuckerman, B., Song, I., & Webb, R. A. 2001b, ApJ, 559, 388
Zuckerman, B., & Webb, R. A. 2000, ApJ, 535, 959